PREPARATION AND CHARACTERIZATION OF NEW RARE EARTH PHOSPHATES AND BOROPHOSPHATES

by

GÜLDEN ÖZEN KAHVECİ

THESIS SUBMITTED TO

THE GRADUATE SCHOOL OF NATURAL AND APPLIED SCIENCES

OF

THE ABANT İZZET BAYSAL UNIVERSITY

IN PARTIAL FULFILLMENT OF THE REQUIREMENTS FOR THE

DEGREE OF

MASTER OF SCIENCE

IN

THE DEPARTMENT OF CHEMISTRY

SEPTEMBER 2005

Approval of the Graduate School of Natural Sciences

Prof.Dr. Davut KÖŞKER

Director

I certify that this thesis satisfies all the requirements as a thesis for the degree of Master of Science.

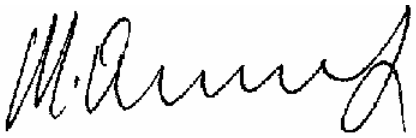

Prof.dr. Mahmut ACIMIŞ

Head of Chemistry Department

This is to certify that we have read this thesis and in our opinion it is fully adequate, in scope and quality as a thesis for the degree of Master of Science.

Assoc. Prof. Dr. Ayşe MORKAN

Supervisor

Examining Committee Members

1. Assoc. Prof. Dr. Orhan TÜRKOĞLU
2. Assoc. Prof. Dr. Ayşe MORKAN
3. Asist. Prof. Dr. Halil GÜLER

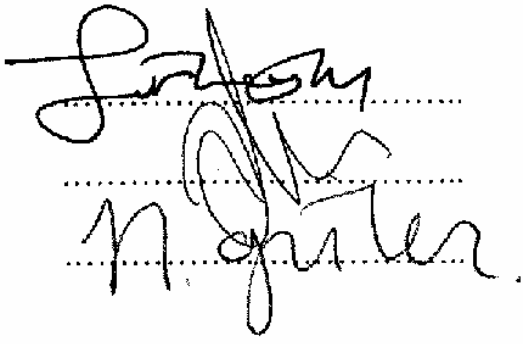

ABSTRACT

PREPARATION AND CHARACTERIZATION OF NEW RARE EARTH PHOSPHATES AND BOROPHOSPHATES

Özen Kahveci, Gülden

Master of Science, Department of Chemistry

Supervisor: Assoc. Prof. Dr. Ayşe MORKAN

September 2005, 82 pages

In the first part of this work, the synthesis of $NaLnP_2O_7.xH_2O$ (Ln: Nd, Gd, Dy, Er, Yb) compounds which were not reported before, were investigated by using solution reactions. The products were analyzed by thermal analysis (TG-DTG, DSC), X-ray diffraction (XRD) and infrared spectroscopy (IR) methods.

The crystal water of these products were found between 4-5 moles by using TG analysis. The products were heated at different temperatures to obtain anhydrous diphosphate compounds. From these compounds, $NaNdP_2O_7$ which was obtained at 650^oC, was indexed in the orthorhombic crystal system and its refined unit cell parameters were calculated as a = 12.579 (7), b = 15.10(1) and c = 16.03 (1) Å.

It was not possible to prepare the dehydrated $NaGdP_2O_7$ compound. After heating period; hydrated $NaGdP_2O_7$ compound was decomposed to $GdPO_4$, $Gd_2P_4O_{13}$ and $HGdP_2O_7$ compounds.

On the other hand, dehydrated pseudo-$NaDyP_2O_7$ and $NaErP_2O_7$ compounds were obtained at 550^oC. The product of dehydrated crystalline $NaYbP_2O_7$ was observed at 500^oC.

In the second part of this work, the $LnBP_2O_8$ (Ln=Nd, Gd, Dy, Er and Yb) compounds were prepared through solid state reactions. It was found that, Nd and Gd borophosphates have monazite structure, Dy, Er and Yb borophosphates have xenotime structure.

In this thesis, the existence of $P_2O_7^{4-}$, PO_4^{3-} and BO_4 units for the obtained products were investigated by using IR spectroscopy method.

Keywords: Phosphate, borate, borophosphate, diphosphate, lanthanide diphosphate, lanthanide borophosphate, xenotime, monazite, XRD, IR, thermal analysis.

ÖZET

YENİ NADİR TOPRAK METALİ FOSFAT VE BORFOSFAT BİLEŞİKLERİNİN HAZIRLANMASI VE KARAKTERİZASYONU

Özen Kahveci, Gülden

Yüksek Lisans, Kimya Bölümü

Tez danışmanı: Doç. Dr. Ayşe MORKAN

Eylül 2005, 82 sayfa

Bu çalışmanın ilk kısmında daha önce rapor edilmemiş $NaLnP_2O_7.xH_2O$ (Ln: Nd, Gd, Dy, Er, Yb) bileşiklerinin sentezi, çözelti reaksiyonları kullanılarak araştırıldı. Elde edilen ürünler, termal analiz (TG-DTG, DSC), XRD ve IR yöntemleri ile incelendi.

TG analiz yöntemi kullanılarak hidratlı ürünlerin kristal sularının,4-5 mol arasında olduğu saptandı. Susuz difosfat bileşiklerinin eldesi için ürünler değişik sıcaklıklarda ısıtıldı. Bu bileşiklerden, 650^oC de elde edilen $NaNdP_2O_7$ bileşiği, ortorombik kristal sistemde indekslenerek, birim hücre boyutları a = 12.579 (7), b = 15.10(1) ve c = 16.03 (1) Å olarak hesaplandı.

Susuz $NaGdP_2O_7$ bileşiğini ise hazırlamak mümkün olmadı. Sulu $NaGdP_2O_7$ bileşiğinin ısıtma işlemleri sonunda $GdPO_4$, $Gd_2P_4O_{13}$, ve $HGdP_2O_7$ bileşiklerine bozulduğu görüldü. Diğer taraftan susuz sahte-$NaDyP_2O_7$ ve $NaErP_2O_7$ bileşikleri

550^{o}C de elde edildi. Susuz $NaYbP_2O_7$ bileşiği ise 500^{o}C de toz kristal olarak gözlendi.

Bu çalışmanın ikinci kısmında $LnBP_2O_8$ bileşikleri, katı-hal reaksiyonları ile hazırlandı. Bunlardan Nd ve Gd borfosfatlarının monazite; Dy, Er, ve Yb borfosfatlarının ise xenotime yapısında oldukları görüldü.

Bu tezde, elde edilen bileşiklerdeki $P_2O_7^{4-}$, PO_4^{3-} ve BO_4 birimlerinin varlığı IR spektroskopisi yöntemi kullanılarak incelendi.

Anahtar kelimeler: Fosfat, borat, borfosfat, difosfat, lantanit difosfat, lantanit borfosfat, xenotime, monazite, XRD, IR, termal analiz.

To My Family…

ACKNOWLEDGEMENT

I'm most grateful to thank my supervisor, Assoc. Prof. Dr. Ayşe MORKAN for her continous encouragement, critical discussion and patience at every stage of this thesis.

I would like to thank my friends Research Asistants Sevim DEMİRÖZÜ ŞENOL and Çiğdem TUÇ for their helps.

I'm grateful to my parents Gönül and Hasan ÖZEN for their support by all means.

I would like to express my thanks to my husband, Mahir KAHVECİ for his moral support and computing the thesis.

Finally, I would like to thank to AİBU-AFP No. 00.03.03.77 and 04.03.03.203 for supporting this work and also acknowledge the Volkswagen Foundation for their support for installing a computerized X-ray powder diffractometer (Hüber) in METU, Chemistry Department.

TABLE OF CONTENTS

LIST OF TABLES

LIST OF FIGURES

CHAPTER I

INTRODUCTION

1.1. X-Ray Diffraction

X-ray diffraction methods are some of the most powerful characterization tools known to scientists. In chemistry and particularly in laboratory experiments concerning solids, the two primary pieces of information most often sought are the structure of the material and its reactivity.

The structures of materials are readily studied by diffraction methods. Structural properties are often responsible for several physical and chemical properties such as electrical conductivity, chemical stability, toughness and others. Presently there is considerable interest in the modification of physical properties by selection of molecular design and by control of structure.

X-ray diffraction methods can be used to study single crystals, powders and other forms of solids.

The relationship in a cubic system between the interplanar distance, d, and the unit cell length, a, and the different Miller indices for different planes, hkl, is the following:

$$\frac{1}{d^2} = \frac{(h^2 + k^2 + l^2)}{a^2}$$

since other systems have different lenghts in their unit cells and different angles between these axes (different than 90^o for the cubic system) other relationships between d, hkl and a, b, and c will be more complicated.

In any set of planes, hkl, Bragg showed that X-rays could diffract from different planes only if diffraction occured between planes having a difference of integral numbers of wavelengths. This relationship can readily be obtained from the following diagram:

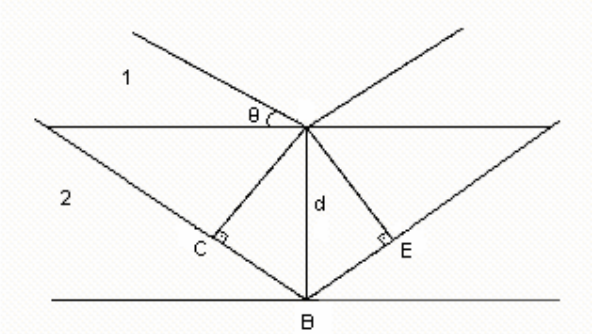

$$\sin\theta = \frac{BC}{d} = \frac{BE}{d}$$

$$n\lambda = BC + BE$$

$$n\lambda = d.\sin\theta + d.\sin\theta$$

$$n\lambda = 2\,d.\sin\theta$$

Bragg's Law

In this case wave 1 diffracts at angle θ intersects the surface or plane 1 at A. Wave 2 diffracts and intersects plane 2 at point B. By drawing right triangles between CAB and EAB are both θ. The spacing between planes 1 and 2 is d. With these two triangles they can be shown that:

$$\sin\theta = \frac{CB}{d} \quad \text{and} \quad \sin\theta = \frac{BE}{d}$$

Wave 2 travels a distance CB + BE farther than wave 1. Bragg's law, therefore, states that there must be an integral number of wavelengths for this extra distance:

$$n\lambda = 2\,d.\sin\theta$$

X-Ray Powder Diffraction

X-ray powder diffraction methods can be used to study the degree of crystallinity of a material, to determine the basic structure of the material, and to tell whether a material is pure or at times whether it has amorphous impurities. The presence of an amorphous impurity can sometimes be verified by a broad weak background peak centered near 25^{o} 2θ. X-rays are produced in the X-ray tube and are collimated onto a sample. In most cases CuKα radiation is used for studies of powders. The sample is usually moved at angles between 10 degrees 2θ to 90 degrees 2θ larger. A proportional counter is used as a detector and the intensities of the diffraction peaks are recorded on a chart recorder or stored in a computer.

A random orientation of the powder is needed in order to observe all of the diffraction peaks. Once the 2-theta values are collected they can be converted to theta and by using Bragg's law values of the d spacings can be obtained. If the substance is a common one then the experimental X-ray powder diffraction pattern can be compared to known published patterns such as those found in the ASTM (American Society for Testing Materials) tables. If a powder pattern has never been collected before, analogies to known structural types can be made.

Thin films, wires, fibers and other similar forms of materials can also be studied with the X-ray powder diffraction method. Usually the powder or other sample form is attached to a glass slide by some noncrystalline material such as vaseline. It is important to not press the sample onto such a slide because a random orientation is necessary in order to observe all of the different planes. During the analysis it is important to compare the peak positions, relative intensities and the general shape of the background signal.

1.2. Infrared Spectroscopy

Absorption of radiation in the vibrational energy of molecules. Energy changes are typically 6 x 10^3 to 42 x 10^3 J mol^{-1}, which corresponds to 250 to 4000 cm^{-1} (2.5 to 40 μm), although some occur between 4000 $^{-1}$ and the begining of the visible region at about 12500 cm^{-1} (0.8 μm or 800 nm) in a region known as the near infrared (NIR). A molecule can absorb energy only if there is a net change in the dipole moment during a particular vibration, a condition fullfilled by virtually all polyatomic molecules. The absorption spectra of such molecules are often very complex and the underlying reason for this complexity is best understood by first considering the spectrum of a heteronuclear diatomic molecule in the gaseous state.

Solids that cannot be dissolved in an infrared-transparent solvent can be suspended in a suitable nonabsorbing liquid medium to form a two-phase mixture called a mull. An essential condition for the acquisition of the satisfactory spectra is that the particle size of the suspended solid be smaller than the wavelength of the infrared beam; if this condition is not realized, a significant portion of the radiation is lost to scattering.

Two techniques are employed. In one, 2 to 5 mg of the finely ground sample (particle size <2 μm) is further ground in the presence of one or two drops of a heavy hydrocarbon oil (Nujol). If hydrocarbon bands are likely to interfere, fluorolube, a halogenated polymer can be used. In either case, the resulting mull is then examined as a film between flat salt plates.

In the second technique, a miligram or less of the finely ground sample is intimately mixed with about 100 mg of dried potassium bromide powder. Mixing can be carried out with a mortar and pestle; a small ball mill is more satisfactory, however. The mixture is then pressed in a special die at 10000 to 15000 pounds per

square inch to yield a transparent disk. Best results are obtained if the disk is formed in a vacuum to eliminate occluded air. The disk is then held in the instrument beam for spectroscopic examination. The resulting spectra frequently exhibit bands at 2.9 and 6.1 μm (3400 and 1600 cm^{-1}) due to absorbed moisture.

Fourier Transform Infrared Spectroscopy (FTIR) is more an instrumental capability rather than a technique. A fourier transform instrument is capable of scanning the sample thousands of times. Very weak signals can thus be separated from the noise by a built-in computer. Part of the power of the FTIR instrument is that it is able to scan the whole spectral output without the use of a slit to examine one small wavelength increment at a time. In addition to its ability to improve the signal to noise ratio by multiple scanning, the optics are inherently simpler leading to better signals compared to the older instruments. FTIR is useful in studying a minor component present as an impurity, or formed as a by-product, or formed as an unfavorable component in an equilibrium process.

1.3. Thermal Analysis Techniques

Thermal analysis is to measure of physical properties of a sample as a function of temperature or a method where the heat absorbed or released by a reaction is traced.

Thermal analysis techniques are used to measure the physical and reactive properties of materials as functions of temperature. Conventional thermal analysis depends on the observation that a phase change produces either an absorption or evaluation of heat. For the case where a pure melt solidifies, the solidification will start at a characteristic temperature. The freezing process is accompained by an evaluation of heat and the rate of this process is related to the rate of heat loss.

Thermal analysis techniques are Thermo Gravimetric Analysis (TGA), Differential Thermal Analysis (DTA), Differential Scanning Calorimetry (DSC), thermometric titration and direct injection enthalpy. In this study, we used Thermo Gravimetric Analysis (TGA) and Differential Scanning Calorimetry (DSC).

1.3.1. Thermo Gravimetric Analysis (TGA)

In a thermogravimetric analysis, change in mass of sample is measured with increasing temperature. This temperature versus mass plot is called thermogram. Any case involving the mass change is investigated by TG. The general reason of the change of mass is removing the volatile compounds water or dissociation of the substance. The phase changes which does not cause the change in mass, like melting can not investigated by TG.

The mass changes directly depend on the stochiometry of reaction. As well as quantitative analysis of the samples which have known qualitative composition can be done, the compositions of new compounds can be estimated.

Thermogravimetric analysis involves weighing a material with a sensitive balance as the temperature is varied in a controlled manner. The signal from a thermocouple measuring the sample temperature is fed into one axis of an x-y recorder. In a TGA instrument with an optical sensor, any change in the beam position is detected optically by a photomultipler tube. This signal is transmitted to an amplifier which provides a current to a feed back coil which acts to maintain the position of the balance beam. The amplifier, in addition to providing the current necessary to maintain the position of the balance beam also sends a signal to the other axis of the x-y recorder. Any weight changes which take place during the heating process are thus recorded as a function of the temperature.

1.3.2. Differential Scanning Calorimetry (DSC)

Differential Scanning Calorimetry is similar to differential thermal analysis. Instead of measuring the difference in temperature between the sample and a reference material as is done with DTA, DSC measures the heat flow into the sample and the reference. Whereas DTA measures differences in temperature, DSC measures differences in energy.

Two different approaches are used to obtain DSC information. One is the power compensated DSC and the other is heat flux DSC. In the former, the sample and the reference are heated by two seperate heaters which are controlled such that the temperatures of the sample and reference are kept constant while the instrument temperature is increased or decreased linearly. The difference in the energy flow necessary to keep the sample and reference at constant temperature is, therefore, determined. In a heat flux DSC, the heat flow into the sample and reference is measured directly. Chromel disks are placed on the bottom of the sample and reference pans. These pans are then placed on a constantan platform. The chromel disk and the constantan disk form a sheet thermocouple. The differential heat flow is proportional to the difference in output from the two sheet thermocouples.

DSC has been used to determine the melting point and enthalpies of fusion of eutectic salt mixtures. It has also been used to determine the eutectic of binary alloy systems.

The changes in quartz and dolomite in cement manufacture has been studied using DSC.

Most of the experiments which give results using DTA can also be determined using DSC. Because of the information obtained by DSC, it has become the method of choice for much of thermal analysis.

1.4. Phosphates

The first uses of phosphates were fertilizers, baking powders and silk whitening. Both disodium phosphate and sodium tripolyphosphate were used cure hams. Many toothpaste contain a phosphate as a polishing agent, usually dicalcium phosphate dihydrate. Phosphate compounds are very important in ceramic industry, cleaners and detergent industry. The most widely used phosphates for cleaners, detergents, dispersants are sodium phophates.

1.4.1. Basic Principles of Phosphate Structure

By definition, the phosphates are those compounds of phosphorus in the anions of which each atom of phosphorus is surrounded by four oxygen atoms arranged at corners of a tetrahedron. There are only several building blocks from which phosphates can be made. One of them is the PO_4 group in which three oxygen atoms are shared with neighboring PO_4 groups. This is called a “branching point”.

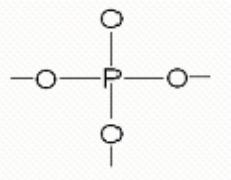

branching point

Another is the PO_4 group in which two oxygen atoms are shared with neighboring groups, and there is only one negative charge or ester linkage. This is called a “middle PO_4 group”.

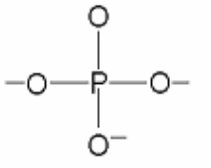

middle group

Then, we have the "end PO_4 group" in which one oxygen is shared, and there are two negative charges or ester linkages. Finally, there is the single (ortho or monophosphate) PO_4 group in which there are three negative charges or ester linkages.

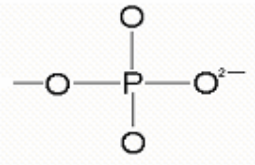

end group

1.4.2. Classification of Phosphates

Like in all classes of compounds in which the anionic part can condense, the classification of phosphates must be supported by the knowledge of the various geometries of the anions.

Phosphate can be classified into four groups:

- Monophosphates
- Condensed phosphates
- Adducts
- Heteropolyphosphates

a) *Monophosphates*

Monophosphates are the compounds of phosphorus where each phosphorus atom is surrounded by four oxygen atoms at the corners of a tetrahedron. Such as M_3PO_4 if M is a monovalent ion.

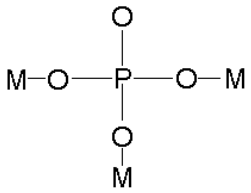

the monophosphates, M_3PO_4

b) ***Condensed Phosphates***

These types of phosphates can be divided in to three subgroups:

- ***Polyphosphates***

The general formula for such anions is given by;

$$P_nO_{3n+1}^{(n+2)}$$

Where n is the number of phosphorus atoms in the anionic entity. The first terms of this condensation, corresponding to a small n, are commonly named oligophosphate (n=2; pyrophosphate $[P_2O_7]^{4-}$, n=3; tripolyphosphate $[P_3O_{10}]^{5-}$, n=4; tetrapolyphosphate $[P_4O_{13}]^{6-}$).

- ***Cyclophosphates***

All simple ring phosphate ions have the true metaphosphate composition $P_nO_{3n}^{n-}$ in which n, can, in principle, have any value Fig.1.1. The presence of ring structures with n = 3, 4, 5, 6 and 8 has been firmly established in various crystalline metaphosphate salts.

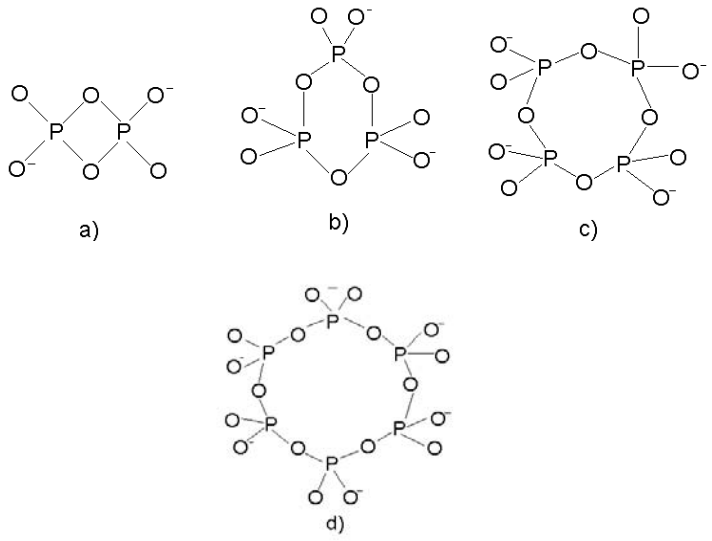

Figure 1.1 *The structures of some cyclophosphates: a) dimetaphosphate b)trimetaphosphate c)tetrametaphosphate d)hexametaphosphate*

- ***Ultraphosphates***

A classification of ultraphosphates on the basis of geometrical type would be very complicated and is unnecessary until more structures have been established. It is more convenient to consider ultraphosphate anions in relation to the formula.

$$[P_nO_{3n+p}]^{(n+2p)}$$

1.5. Pyrophosphates

The pyrophosphate (diphosphate) ion, $P_2O_7^{4-}$, represents the simplest condensed phosphate. It can be made by heating acid orthophosphates when condensation takes place and water is eliminated Fig.1.2.

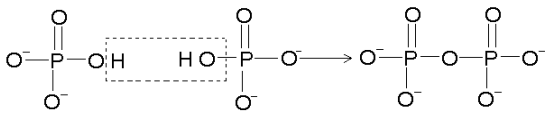

Figure 1.2 *Formation of pyrophosphate*

The two basic features of structural importance are (i) the angle at the central shared O atom (angle P/O/P) and (ii) the relative orientation of the two tetrahedra involved.

In Fig.1.3 are shown the more symmetrical rotational isomers, with a central P/O/P angle of 180° (linear) and with a P/O/P angle of <180° (nonlinear).

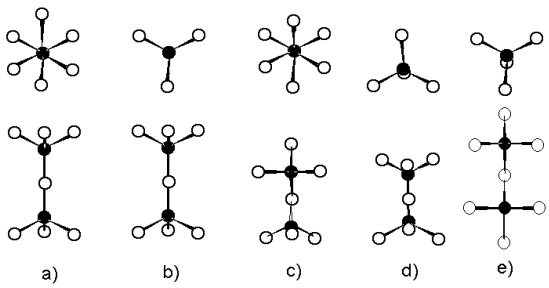

Figure 1.3 *Schemes of symmetrical orientation of adjacent tetrahedra in condensed phosphates.* ***(a)****linear trans (P/O/P=180°),* ***(b)****linear cis (P/O/P=180°),* ***(c)****non-linear trans(P/O/P<180°),* ***(d)****non-linear α-cis (P/O/P<180°),* ***(e)****linear β-cis (P/O/P<180°)*

Structure determinations of a number of pyrophosphate salts have shown that both linear (straight) and non-linear (bent) ions can exist, with a value of P/O/P in the range 130-180^{o}. Both "cis" (eclipsed) and somewhat less symmetrical rotational isomers have been found amongst pyrophophates. There is evidence from IR and Raman spectra for the existence of rotational isomers in solution.

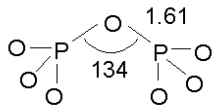

Investigations of the structure of $Na_4P_2O_7$.$10H_2O$ have shown the anion has a two fold symmetry axis with an approximate trans orientation of the two tetrahedra involved. The P/O/P angle is 130^{o} and the configuration resembles that in figure. The iner P-O-P bond lengths are 1.612 $\pm$ 0.005 Å and the terminal P-O bond lenghts are 1.523 $\pm$ 0.004 Å. The sodium ions in this structure are octahedrally coordinated as $NaO_2(H_2O)_4$ and $Na(H_2O)_6$ groups which combine to form sheets paralel to (100). These sheets are cross-linked via the pyrophophate groups.

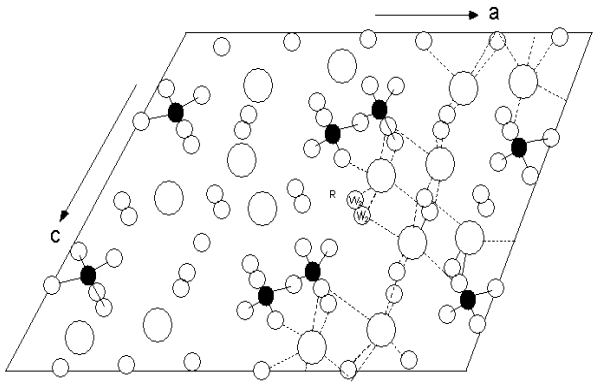

Figure 1.4 *Pyrophosphate structure of $Na_4P_2O_7$.$10H_2O$ in [b] projection. Filled circles represent P atoms and concentric circles represent pairs of oxygen atoms related by mirror planes.*

Phosphates of the rare earth elements are very important in chemistry and technology because of their main form of the occurrence in nature. Giesbrecht and Perrier [1] claimed to have obtained $NaCeP_2O_7.4.5H_2O$ by adding sodium diphosphate solution to a solution of cerium (III) chloride, without mentioning the pH of the solution. Kızılyallı et al. [2] applied the same method for the preparation of $NaGdP_2O_7.4.5H_2O$ however, the chemical analysis of the product heated at 700°C, showed that it contained only 0.11 % of Na_2O whereas the theoretical percentage of Na_2O in $NaGdP_2O_7$ is 8.71 %. Therefore, it was concluded that this compound was in fact hydrogen gadolinium diphosphate retaining some alkali metal as impurity by characterizing its X-ray powder diffraction and IR data. Later on, the single crystals of this compound have been also synthesized, and their structure was solved in the triclinic system [3]. Then, characterization and thermal behavior of the same compound has been reported, and also the single crystal structure of this compound has been reported [4]. Most recently, acid rare-earth phosphates have been prepared by using the same method in which the solution of sodium diphosphate and the acidic solution of the rare-earth chloride were mixed [5].

Some double diphosphates of rare earths have been synthesized by several researchers [1, 6, 7]. Tananev et al. [8] reported the preparation of some rare earth alkali double diphosphates through solution reactions and complex X-ray powder diffraction patterns in the case of $LiLaP_2O_7$, $KLaP_2O_7$ and α- and β-$NaLaP_2O_7$ without indexing. Later on, Anisimova et al. [9] prepared double diphosphates of the type $NaLnP_2O_7$ (Ln= La, ... Lu) by using Ln_2O_3 and vitreous $NaPO_3$ and annealing the mixed powders for 50 hours. According to the crystal-chemical parameters of the products obtained, $NaNdP_2O_7$ and $NaGdP_2O_7$ were indexed in monoclinic system whereas $NaCeP_2O_7$ was in the orthorhombic system. They also found that when the

double diphosphate is heated at 790°C it decomposed in the solid phase as shown in the following reaction,

$NaNdP_2O_7$ (cryst) → $NdPO_4$ (cryst.) + $NaPO_3$ (amorph)

But, they have not studied the IR spectra of these compounds.

Quite recently, $NaGdP_2O_7$ has been prepared using the following solid-state reactions by Kızılyallı and Darras [10].

$Gd_2O_3 + 4\ (NH_4)_2HPO_4 + Na_2CO_3 \rightarrow 2NaGdP_2O_7 + CO_2 + 8NH_3 + 6H_2O$

$Gd_2O_3 + 2\ P_2O_5 + Na_2CO_3 \rightarrow 2\ NaGdP_2O_7 + CO_2$

$GdPO_4 + NaPO_3 \rightarrow NaGdP_2O_7$

In these reactions to avoid the decomposition of $NaGdP_2O_7$ at most care was taken and the temperature was kept around 650°C. The XRD powder data is indexed in the orthorhombic system with the approximate unit cell dimentions of a=12.44, b=15.00, c=15.87 Å and the space group was found to be Pmm2. Analysis of the vibrations of $P_2O_7^{4-}$ ion according to C_{2v} symmetry and band assignments for IR and Raman spectra were also reported. The P-O-P band was found to be non linear and coincidenses in the IR and Raman spectra suggested that the most probable space group is noncentrosymmetric.

Single crystal structure of $NaEuP_2O_7$ has been grown by the flux technique and characterized by X-ray diffraction [11]. Then, an other diphosphate $NaLaP_2O_7$ has been synthesized. It's structural characterization has been made by X-ray diffraction, raman and infrared spectroscopy[12]. This compound crystallizes in the orthorhombic Pnma space group with the following unit cell dimensions: a=8.645(2), b=5.317(1), c=12.737(2) Å, V=585.5(2) Å, Z=4.

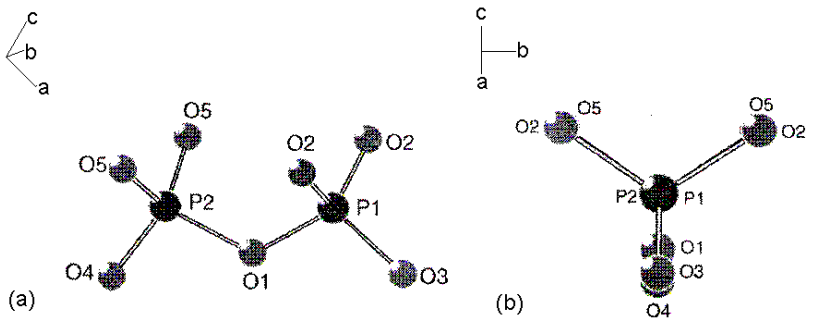

Figure 1.5 *Projection of the P_2O_7 group in the ($P_1O_1P_2$) plan (a) and along the P_1-P_2 direction (b).*

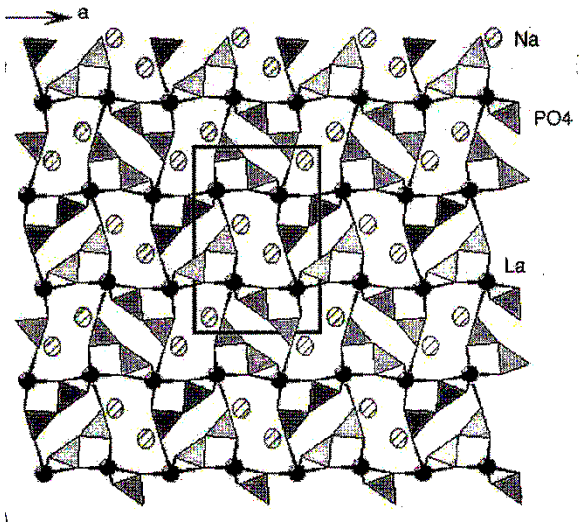

Figure 1.6 *Projection along **b**-direction, of the atomic arrangement in $NaLaP_2O_7$.*

In order to investigate the effect of multiphonons on the radiative process of rare eart ions, a new pseudo-pyrophosphate (PPP) with formula $NaDyP_2O_7$ was synthesized via solid-state reaction, and characterized by X-ray powder diffraction, infrared and raman spectra [13].

Later on; raman and infrared absorption spectra of diphosphates $CsLnP_2O_7$ (Ln: Gd, Tb, Dy, Ho, Y, Er, Tm, Yb) have been recorded and interpreted using factor group analysis [14].

1.6. Borophosphates

Borophosphate is a copolymer of borontrioxide and phosphor pentoxide which are water-soluble and have low melting points. Structure of BPO_4 is similar to silica, act as host lattices for small charge-balanced quantities of other metal oxides, forming isotypic mixed phases which are higly coloured and have pigmentary value.

BPO_4 has silica type structures; which are quartz and low cristobalite forms.

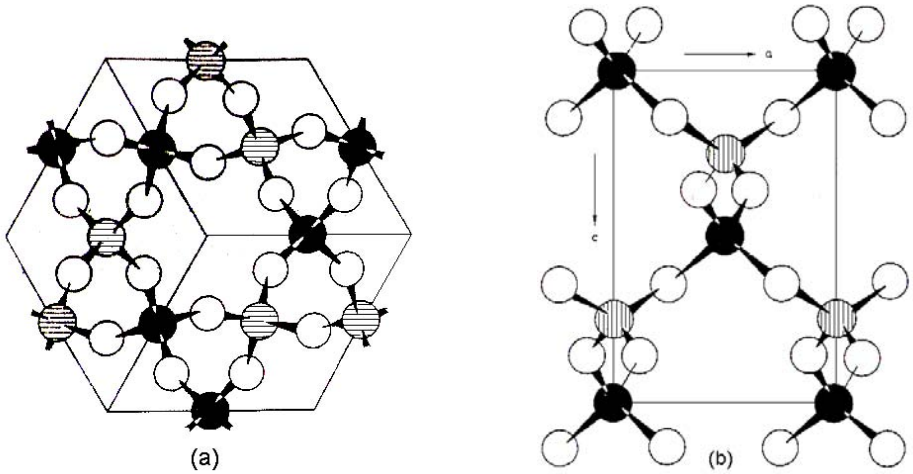

Figure 1.7 *Silica type structuıres.* ***(a)*** *Quartz, c axis projection;* ***(b)*** *Cristobalite, a axis projection; structures drawn with alternate Si atoms shaded differently to indicate ABO_4^- type structures. Networks with lower symmetry than the parrent silica structure are produced by the replacement of silicon by atoms of two different kinds. This may necessitate a space group of lower symmetry or a doubled unit cell axis unless some kind of statical arrangement of the atoms A and B is adopted.*

The P-O and B-O bond lenghts are not equal to each other. P-O = 1.55 Å and B-O = 1.44 Å. Both the phosphorous and the boron atoms are tetrahedral.

$Ca[BPO_5]$, and $Sr[BPO_5]$ were obtained as single-phase microcrystalline powders in platinum crucible at 900°C by Kniep et al. [15] and Gözel [16].

$$CaHPO_4 . 2H_2O + H_3BO_3 \rightarrow Ca[BPO_5] + 4H_2O$$

$$SrCO_3 + H_3BO_3 + (NH_4)_2HPO_4 \rightarrow Sr[BPO_5] + 3H_2O + 2NH_3 + CO_2$$

Recently with the system of $M^I_2O/M^{II}O$-B_2O_3-P_2O_5, another study was done for Ba by Sedmale et al. [17]. But in this case, they tried to synthesize borophosphate glass composed of BaO-B_2O_3-P_2O_5. Shi Y. et al. [18] studied the crystal structure and thermal decomposition process of $BaBPO_5$ by X-ray diffraction and vibration spectroscopic techniques and showed that its decomposition products are $BaBP_3O_{12}$ and $Ba_2P_2O_7$. The structure of $BaBPO_5$ is refined by Rietveld technique, which indicates that the structural units of this compound are PO_4 and BO_4 tetrahedra as well as irregular rare earth polyhedra.

Two compounds Li, Ba-nanoborate $LiBaB_9O_{15}$ (I) and Ba-borophosphate $BaBPO_5$ (II) were synthesized in the hydrothermal systems $BaCl_2$-Li_2CO_3-B_2O_3-H_2O and BaO-B_2O_3-P_2O_5-H_2O (T=280°C, P=100 bar, 20 days)[19].

Alkaline-earth borophosphates are interesting solid-state materials which have an isoelectronic relationship with silicates. These materials are biocompatible with the living body, so they are called bioceramics. The crystal structure of these alkaline-earth borophosphates has been solved and reported by Kniep [15] and Gözel [16] et al.

Most of the best-known materials with optical and electro-optical applications are either borates or phophates [20]. Names such as BBO (β-BaB_2O_4)

[21], LBO (LiB_3O_5) [22], KTP ($KTiOPO_4$) and KDP (KH_2PO_4) [23] are well-known commercially and are heavily used industrially for making a range of different optical elements. In the last couple of years, the first few compounds combining both borate and phosphate groups were synthesized and structurally characterized. High temperature synthesis have produced a handful of metal borophosphates, all of main group metals.

$CaBPO_5$ was synthesized by different solid state reactions than reported before and its X-ray powder diffraction and IR data were reported [24,25]. $SrBPO_5$ was synthesized by a solid-state reaction reported [26] and by a new solid state reaction using BPO_4 as a phosphating agent. It was also obtained by a hydrothermal method. The structure of the compound was solved by Rietveld analysis before. The examination of X-ray powder diffraction data showed that, $SrBPO_5$ is isostructural with $CaBPO_5$ and $BaBPO_5$.

Single crystals of $Co_3[BPO_7]$ were obtained by boron flux method and characterized by single crystal diffraction data [27]. Another research; α-$Mg_3[BPO_7]$ (low temperature form) which is isostructural with $Zn_3[BPO_7]$ has been sythesized by the solid-state reactions of $MgHPO_4.H_2O$ with $MgCO_3$ and H_3BO_3 at 1200^{o}C, $Mg_3B_2O_6$ with $MgCO_3$ and $(NH_4)_2HPO_4$ at 1100^{o}C, and MgO with B_2O_3 and P_2O_5 at 1100^{o}C with the molar ratios of 1:2:1, 1:3:2 and 6:1:1, recpectively [28]. Nonhygroscopic single crystals of β-$Zn_3[BPO_7]$ have been grown from the stoichiometric melt and characterized as a nonlinear optical crystal [29]. The phase transition of β-$Zn_3[BPO_7]$ into α-$Zn_3[BPO_7]$ is effectively suppressed by the appropriate heat treatment.

$NaMg(H_2O)_2[BP_2O_8].H_2O$ and $NH_4Mg(H_2O)_2[BP_2O_8].H_2O$ were synthesized by hydrothermal synthesis and was characterized by X-ray powder diffraction and IR method [30].

Aluminosilicate compounds have been studied because of their applications as catalysts, molecular sieves and ion exchangers [31]. Al^{3+} and Si^{4+} in the zeolite frameworks have been either completely or partially substituted with a variety of atoms. For example, alumino-(or gallo-) phosphates and zinco-(or beryllo-) phosphates or –arsenates have been found to be isotypic with known aluminosilicate molecular sieves [32,33]. Of fundamental importance is the synthesis of new zeolitic materials with novel structural properties because the utility of these crystalline materials is intimately correlated to their geometrical features [34].

The first tetrahedral framework structural borophosphate compounds were synthesized by Kniep et al. [35] zincoborophophates, $K[ZnBP_2O_8]$ and $A[ZnBP_2O_8]$ ($A=NH_4^+,Rb^+,Cs^+$). The topolagies of compounds display a close relationship to tecto-aluminosilicates (feldspar family and gismondine).

The hydrothermal synthesis and single crystal X-ray structural characterization of $Fe(H_2O)_2[BP_2O_8].H_2O$ were reported [36]. It's a hydrated iron borophosphate with a chiral, tetrahedral framework topology.

The solid state experiments of rare earth oxides with boron and phosphorus containing compounds were synthesized [25]. For example; $Nd_7BP_2O_{17}$ was prepared by the solid-state reactions of the components Nd_2O_3, $(NH_4)_2HPO_4$ and H_3BO_3 in the molar ratio of 7:4:2. The following reaction was predicted:

$$7Nd_2O_3(s) + 4(NH_4)_2HPO_4(s) + 2H_3BO_3(s) \rightarrow 2Nd_7BP_2O_{17}(s) + 8NH_3(g) + 9H_2O(g)$$

The reaction was performed at 1000^oC for 64h.

Single-phase samples of the compound $Ba[BPO_5]$ could not be synthesized under the same conditions. Experiments employing an excess of $(NH_4)_2HPO_4$ as a flux medium or a solvent provided single crystals of the new compound $Ba_3[BP_3O_{12}]$.

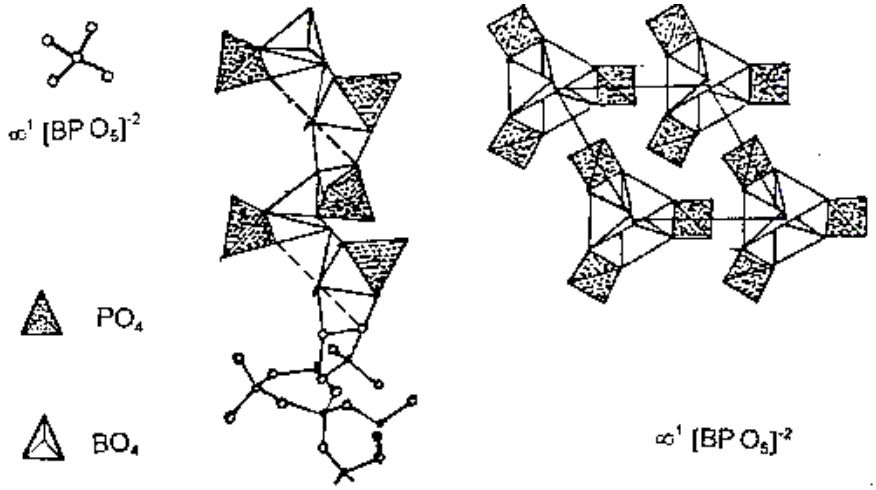

Figure 1.8 *Crystal structures of $Ca[BPO_5]$ and $Sr[BPO_5]$*

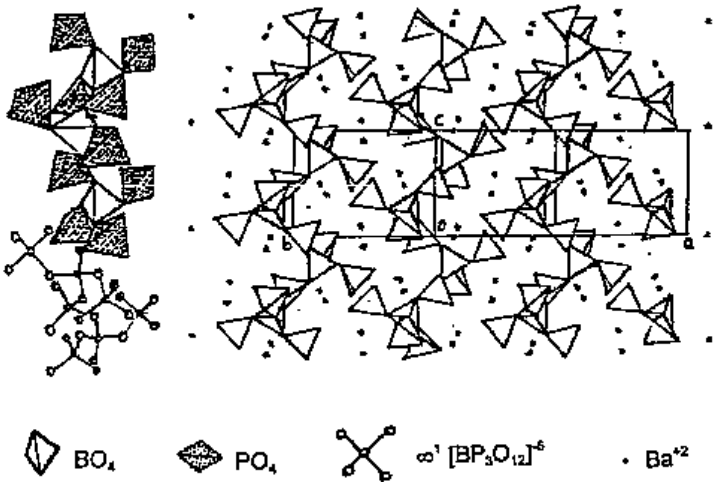

Figure 1.9 *Crystal structure of $Ba_3[BP_3O_{12}]$*

^{11}B and ^{31}P MASS-NMR spectroscopy of three borophosphates was used and then it showed that $CaBPO_5$ and BPO_4 represent nearly pure samples, $SrBPO_5$ contains β-$Sr_2P_2O_7$ as well as BPO_4 as impurities [37].

The crystal structure of the isomorphical rare earth borophosphate compounds, $Ln_7O_6(BO_3)(PO_4)_2$ (Ln = La, Nd, Gd and Dy), has been synthesized by a standard solid-state reaction technique. Then; these isomorphical borophosphate compounds were indexed in monoclinic system [38].

Borophosphates are intermediate compounds of the system M_xO_y-B_2O_3-P_2O_5-(H_2O) which contain complex anionic structures built of BO_4, BO_3 and PO_4 groups and their partially protonated species, respectively. Although systematic investigations of borophosphates have been started only 5 years ago [15,39] numerous borophosphates and their crystal structures have already been reported up to now. A first approach to the development of a structural chemistry of borophosphates is based on the linking principles of the primary building units following the general line of silicate crystal chemistry [40].

The crystal structures of borophosphates are first divided into anhydrous and hydrated phases. Further grandings are based on the molar B:P ratios [41]. Anhydrous borophosphates are listed in Table 1.1.

The crystal structure of α-$Zn_3[BPO_7]$ ($\equiv Zn_3[(BO_3)(PO_4)]$) [42] contains isolated planar BO_3 groups and PO_4 tetrahedra. Trigonal planar borate groups sharing one common oxygen atom with a phosphate tetrahedron as well as isolated phosphate tetrahedra are present in the crystal structure of $Co_5[BP_3O_{14}]$ ($\equiv Co_5[(BPO_6)(PO_4)_2]$) [20]. The tetrahedral chain structures are loop-branched (formation of 3-membered rings: $M[BPO_5]$; M=Ca,Sr [15], M=Pb [43]) and open branched ($M_3[BP_3O_{12}]$; M= Ba [15], M=Pb [44]), respectively.

Anhydrous and hydrated borophosphates with a molar ratio B:P<1, B:P=1 and B:P>1 are given in tables 1.1; 1.2, 1.3 and 1.4 respectively.

Table 1.1. *Anhydrous borophosphates [41]*

Complex Anions	**B[CN]**	**B:P**	**Compound**
Single 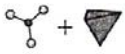	[3]	1	α-$Zn_3[BPO_7]$
Double single 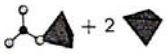	[3]	1 (0,33)	$Co_5[BP_3O_{14}]$
Chains Loop-Branched 	[4]	1	$M[BPO_5]$ M=Ca,Sr M=Pb
Loop-Branched 	[4]	0,66	$Na_5[B_2P_3O_{13}]$
Open-Branched 	[4]	0,33	$M_3[BP_3O_{12}]$ M=Ba M=Pb

Borate tetrahedra and boron atoms, blue; phosphate tetrahedra, red; oxygen of BO_3 groups, gray spheres; CN = coordination number.

Table 1.2. *Hydrated Borophosphates, B:P<1 [41]*

Complex Anions	B[CN]	B:P	Compound
Oligomers			
unbranched triple  *)	[4]	0,5	$NaFe[BP_2O_7(OH)_3]$
open branched ring 	[4]	0,5	$K_2Fe_2[B_2P_4O_{16}(OH)_2]$
loop branched + single 	[4]	0.5 (033)	$Na_4Cu_3[B_2P_4O_{15}(OH)_2].2HPO_4$
loop-branched chain 	[4]	0,5	$M^IM^{II}(H_2O)_2[BP_2O_8]\ .\ H_2O$ M^I= NaK; M^{II}= Mg, Mn, Fe, Co, Ni, Zn
layers 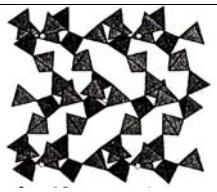 3-and 9-membered rings	[4]	0,66	$Co(C_2N_2H_{10})[B_2P_3O_{12}(OH)]$
 6-and 8-membered rings	[4]	0,5	$Na_{1.89}Ag_{0.11}[BP_2O_7(OH)]$ $Na_2[BP_2O_7(OH)]$

**) protons of the phosphate tetrahedra are involved in a"symmetrical" hydrogen bridge to adjacent oligomers.*

Table 1.3. *Hydrated borophosphates, B:P=1 [41]*

Complex Anions	**B[CN]**	**Compound**
single 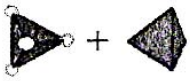	[4]	$Mn_3(OH)_2[B(OH)_4][PO_4]$
double 	[4]	$Mg_3(H_2O)_6[B_2(OH)_6(PO_4)_2]$
unbrached chain 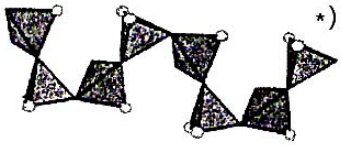	[4]	$Fe[B_2P_2O_7(OH)_5]$
framework 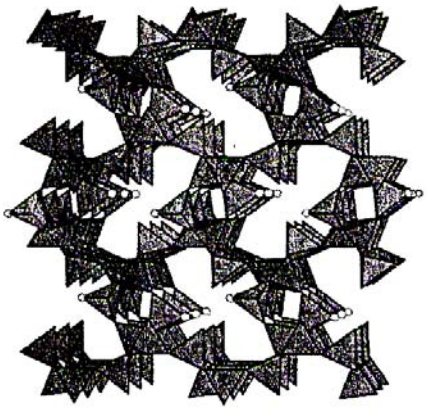 3-,4-,6-,9- and 12- membered rings	[4]	$M[B_2P_2O_8(OH)]$, M=RB,Cs

**) one of the protons of each borate tetrahedron is involved in a"symmetrical" hydrogen bridge to an adjacent chain.*

Table 1.4. *Hydrated borophosphates with a molar ratio B:P>1 [41]*

Complex Anions	B[CN]	B:P	Compound
chains  loop-branched	[3]+[4]	5	$K_3[B_5PO_{10}(OH)_3]$
 open loop-branched	[3]+[4]	3	$Li[B_3PO_6(OH)_3]$
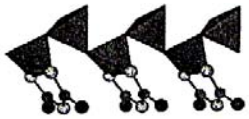 open loop-branched	[3]+[4]	3	$(NH_4)_2[B_3PO_7(OH)_2]$

The chain structures given in Tables 1.1, 1.2, 1.3 and 1.4 show the common principle that all the corners of BO_4 tetrahedra share common corners with neighboring tetrahedra.

On the basis of structural classifications summarized in the Tables 1.1-1.4, the following supplementary principles should be pointed out.

1) Compounds with molar ratio B:P>1 contain boron in 3-fold and tetrahedral coordination.
2) Nonbridging corners of borate species in hydrated phases correspond to OH groups.
3) Analogies to the structural chemistry of borates are also given by the frequent formation of 3-membered rings.

4) P-O-P linking is not observed [41].

BPO_4, which is a very well known compound, is an important catalyst, especially for organic reactions [45]. The other importance of BPO_4 is its usage as a phosphating agent. Vasovic et al. [46] investigated the phosphating feature of BPO_4 to obtain Mg, Ca, Zn and Bp phosphates through solid state reactions of BPO_4 with the corresponding oxides. The strength of porcelain can be considerably improved by the addition of BPO_4 [47]. It is also used as an insulator [48]. Glasses capable of absorbing a substantial portion of electromagnetic radiation contain BPO_4 [49]. Furthermore, in electronic packaging substrate technology, borophosphosilicate glass ceramics have been used in recent years [50-53].

BPO_4 was first prepared from the mixtures of B_2O_3 and $(NH_4)_2HPO_4$ or B_2O_3 and P_2O_5 by solid state synthesis at high temperatures (Tmax =100^oC) [54-59].

The crystal structure contains BO_4 and PO_4 tetrahedra. BPO_4 is a copolymer of two water soluble and low melting oxides: boric oxide and phosphorus oxide. It is insoluble, chemically inert and has a high softenig point. It is a four connective crystalline polymer whose structure (Fig1.10) is similar to that of silica [60].

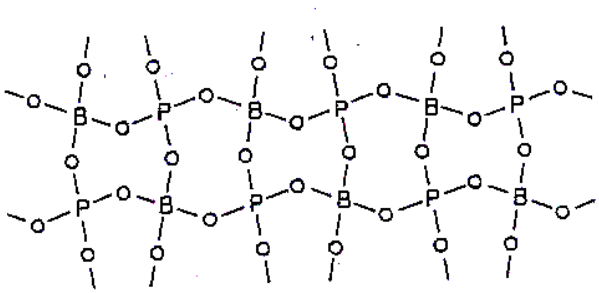

Figure 1.10 *Structure of BPO_4*

Much process has been made in the synthesis of materials by hydrothermal and microwave methods. Conventional techniques such as solid states reactions at high

temperatures or photochemical, catalytic, ultrasonic and high pressure reactions are used to stimulate chemical reactions which proceed slowly under ambient conditions [61]. On the other hand, the use of controlled microwave energy for ceramic processing and drying and for melting silica, alumina and aluminosilicate gels have been reported [62].

Microwave heating techniques have stimulated interest because of their potential advantages, including significant reductions in manufacturing costs [63]. Microwave energy is widely used to process a variety of ceramic materials. The use of microwave plasma produces highly excited electronic states by the decomposition of gaseous species that recombine to give metastable phases. Kamo et al. [64] synthesized diamond depending on this principle.

There are many advantages of microwave processing over conventional processing methods [62,63]. These are; 1) Significant reductions in manufacturing costs due to energy savings and shorter processing times, 2) Improved product uniformity, 3) Improved or unique microstructure and properties, 4) Improved product quality, 5) Very rapid processing (2 to 50 times faster than conventional methods), 6) Capability of high energy concentration in short times and in selected regions, 7) Acceleration of sintering and diffusion and thus densification at lower temperatures.

Fast microwave-assisted reaction for the synthesis of BPO_4 and the preparation of BO_4 by a hydrothermal method was reported [65].

Microwave heating is fundamentally different from conventional processes. In the microwave process, heat is generated internally within the material instead of originating heat. The materials, that can be processed by microwave energy are dielectrics (electrically insulating) such as Al_2O_3, MgO and SiO_2 and most glasses.

They are transparent to microwaves at ambient temperature [63]. Recently, microwave energy was used for the synthesis of inorganic borophosphate materials such as $Na_5[B_2P_3O_{13}]$ [66]. The synthesis of $Na_5[B_2P_3O_{13}]$ took only two minutes to transform a solid mixtures of borate and phosphate hydrates into crystalline title compound.

$Na_5[B_2P_3O_{13}]$ was first prepared from mixtures of $NaH_2PO_4.2H_2O$ and $NaBO_2.4H_2O$ by high temperature synthesis (Tmax=780^oC); the crystal structure (Fig1.11) contains BO_4 and PO_4 tetrahedra which share common vertices to form infinite chain anions $[B_2P_3O_{13}]^{5-}$ running along the [100] direction of the monoclinic crystal structure [67].

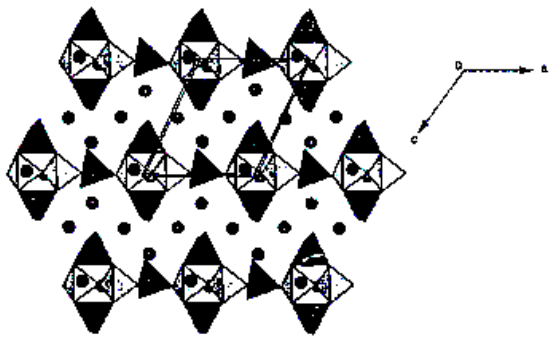

Figure 1.11 *Crystal structure of $Na_5[B_2P_3O_{13}]$*

The basic idea for a microwave-asisted preparation of borophosphates is consistent with the observation of high microwave susceptibilities of those phosphate and borate hydrates [68,69] which are used as adduct materials.

1.7. Boron and Phosphate Reserves in Turkey

Turkey has the largest boron reserves in the world. The total B_2O_3 reserves in the world's %63 are in Turkey as given in Table 1.5.

Table 1.5. *Boron reserves of Some Countries [70]*

Countries	**Reserve(1000 tones)**	**%B_2O_3**
Turkey	803,000	63
USA	209,000	16.4
USSR	136.000	10.7
Chile	41.000	3.2
China	36.000	2.8
Peru	22.000	1.7
Bolivia	19.000	1.5
Argentina	9.000	0.7
Total	**1.323.000**	**100**

The mineralogical properties of important boron minerals present in Turkey are [71]:

Colemanite ($2CaO.3B_2O_3.5H_2O$)

Pandermite ($5CaO.6B_2O_3.9H_2O$)

Borax ($Na_2O.2B_2O_3.10H_2O$)

Ulexite ($Na_2O.2CaO.\ 5B_2O_316H_2O$)

Boracite ($6MgO.8B_2O_3.MgCl_2$)

Meyerhofferite ($2CaO.3B_2O_3.7H_2O$)

Phosphate rock is widely distributed in the former CENTO region (Iran, Pakistan and Turkey) occurring chiefly in rocks.

Phosphate rock is of widespread occurrence in Turkey but only deposits in southeastern Turkey, in the Derik-Mazıdağı region of Mardin Province, are of potential economic importance as a source of phosphate for fertilizer manufacture [72].

1.8. Purpose of the Work

In this thesis, to synthesize some rare earth phosphates, two different synthesis methods were studied. The aim, in the first part of this work, is to synthesize some rare earth diphosphates by using solution method. Too many researches have been tried on rare earth diphosphate through the solid state reactions up to now. However, in this study, solution reactions of Ln_2O_3 (Ln: Nd, Gd, Dy, Er andYb) with $Na_4P_2O_7$ will be investigated to synthesize $NaLnP_2O_7$ type of diphosphates which were not reported before. The expected reaction of these compounds:

$$LnCl_3(aq) + Na_4P_2O_7(aq) \rightarrow NaLnP_2O_7.xH_2O(s) + 3Na^+(aq) + 3Cl^-(aq)$$

In the last years, the interest of the boron compounds, especially borophosphates increased. Therefore, in the second part of this work, solid-state method will be used to synthesize some rare earth borophosphates. The following solid-state reactions of Ln_2O_3 (Ln: Nd, Gd, Dy, Er andYb) with $NH_4H_2PO_4$ and B_2O_3 will be tried to obtain $LnBP_2O_8$ at different temperatures.

$$Ln_2O_3(s) + 4\ NH_4H_2PO_4(s) + B_2O_3(s) \rightarrow 2LnBP_2O_8(s) + 4NH_3(g) + 6H_2O(s)$$

CHAPTER II

EXPERIMENTAL TECHNIQUES

2.1. Chemicals

The following chemicals were used in the synthesis of the products:

Nd_2O_3: 99.9% pure taken from Fluka

Gd_2O_3: 99.9% pure taken from Fluka

Dy_2O_3: 99.9% pure taken from Fluka

Er_2O_3: 99.9% pure taken from Fluka

Yb_2O_3: 99.9% pure taken from Fluka

$Na_4P_2O_7$: Merck

B_2O_3: Merck

$NH_4H_2PO_4$: Merck

KBr: Spectroscopic grade and it was used for making IR pellets.

It was dried at 180^{o}C about 2 hours before using.

2.2. Instrumentation

i.) X-Ray Powder Diffractometer

X-ray powder diffraction patterns (XRD) were recorded on a Rigaku and CuK_α (30-40 kV, 10-20 mA, λ=1.54056 Å) radiation. NaCl was used as an external standard. Indexing of the XRD pattern was accomplished by a program developed in our laboratory and checked by Huber diffractometer

program. The least square refiment procedure of the unit cell parameters was done by the Huber program.

ii.) Infrared Spectrophotometer

Jasco 430 FT/IR spectrophotometer was used to optain the spectra of the products in the region of the 4000-400 cm^{-1}. Spectra of solid samples were taken from KBr pellets using 0.5:100 (wt/wt) product to KBr ratio.

iii.) Thermogravimetric Analyzer

Thermal analysis records were obtained by using Perkin Elmer Pyris 1 instrument.

iv.) Differential Scanning Calorimeter (DSC)

The energy differences were measured by using Perkin Elmer Pyris 1 instrument.

v.)Furnaces

All the reactions have been carried out in air with the aid of Nuve MF 1400, Nuve 1200 and Alser 1600 furnaces. Heating ranges were 550-1200 ^{o}C.

2.3. Experimental Procedure

2.3.1. Solution Reactions

2.3.1.1. Solution reaction of $NdCl_3 + Na_4P_2O_7$

In this solution method; 25ml portion of 0,09M $NdCl_3$ solution was prepared from dissolution of Nd_2O_3 in dilute HCl solution then pH=1-2 was adjusted. 25ml of 0,09 M $Na_4P_2O_4$ solution was added by stirring. Stirring was continued for hours. After that; gelatinious precipitate was obtained. Then filtered and dried under vacuum at 130 ^{o}C. The thermal behaviours of this product was investigated with TG-DSC. Further heatings were done at 650, 700 and 750^{o}C about 6-7 hours, the

structure of this product was examined by using X-ray powder diffraction and IR analysis. The expected reaction was:

$$NdCl_3(aq) + Na_4P_2O_7\,(aq) \rightarrow NaNdP_2O_7.xH_2O(s) + 3Na^+\,(aq) + 3Cl^-\,(aq)$$

2.3.1.2. Solution reaction of $GdCl_3 + Na_4P_2O_7$

Gd_2O_3 which was taken stoichiometric proportion was dissolved in dilute HCl solution to obtain 0,09 M $GdCl_3$ solution. The pH of the $GdCl_3$ solution was set to 1-2 $Na_4P_2O_7$ solution which was the same molar $GdCl_3$ solution, was added into this solution. It was stirred during 6 hours. The obtained precipitate was filtered and dried at 130^{o}C under vacuum. Then the mixture was heated at 550, 650 and 750^{o}C about 6 hours. The following reaction was expected:

$$GdCl_3(aq) + Na_4P_2O_7\,(aq) \rightarrow NaGdP_2O_7.xH_2O(s) + 3Na^+\,(aq) + 3Cl^-\,(aq)$$

2.3.1.3. Solution reaction of $DyCl_3 + Na_4P_2O_7$

To obtain 0,09M $DyCl_3$ solution, Dy_2O_3 was dissolved in dilute HCl solution, 0,09M $Na_4P_2O_7$ was added with stirring during 6 hours. The mixture was filtered and the obtained precipitate was dried. The heatings were done at 150, 540, 650^{o}C about 6 hours. The following reaction was expected:

$$DyCl_3(aq) + Na_4P_2O_7\,(aq) \rightarrow NaDyP_2O_7.xH_2O(s) + 3Na^+\,(aq) + 3Cl^-\,(aq)$$

2.3.1.4. Solution reaction of $ErCl_3 + Na_4P_2O_7$

Stoichiometrical amounts of Er_2O_3 was taken, to dissolve in dilute HCl 0,09 M $ErCl_3$ solution was formed, then adjusted to pH=1-2 0.09 M $Na_4P_2O_7$ was added in to this solution by stirring. The precipitate was observed and filtered. Then

it was dried under vacuum. The reaction was heated at 150-550 ^{o}C for 6 hours. The expected reaction was:

$$ErCl_3(aq) + Na_4P_2O_7\,(aq) \rightarrow NaErP_2O_7.xH_2O(s) + 3Na^+\,(aq) + 3Cl^-\,(aq)$$

2.3.1.5. Solution reaction of $YbCl_3 + Na_4P_2O_7$

0,09 M $YbCl_3$ solution was obtained from the dissolution of Yb_2O_3 in dilute HCl solution. The pH of this $YbCl_3$ solution was adjusted to 1-2 then into this solution, 0,09 M $Na_4P_2O_7$ was added with stirring. The observed precipitate was filtered and dried, the heatings were done at 150-500^{o}C for hours. The expected reaction was:

$$YbCl_3(aq) + Na_4P_2O_7\,(aq) \rightarrow NaYbP_2O_7.xH_2O(s) + 3Na^+\,(aq) + 3Cl^-\,(aq)$$

2.3.2. Solid-State Reactions

2.3.2.1. Solid-State Reaction of $Nd_2O_3 + B_2O_3 + 4NH_4H_2PO_4$

The reactants were weighed separately and ground together in an agate mortar. Then the reaction was performed at 600^{o}C, 800^{o}C, 900^{o}C, 1000^{o}C, 1100^{o}C and 1200^{o}C in a porcelain crucible for 7 hours. At the end of each heating period and crucible was weighed, the mixture was ground and samples were taken from this mixture for X-ray and IR analysis. The following reaction was predicted:

$$Nd_2O_3(s) + B_2O_3(s) + 4NH_4H_2PO_4(s) \rightarrow 2NdBP_2O_8(s) + 4NH_3(g) + 6H_2O(g)$$

2.3.2.2. Solid-State Reaction of $Gd_2O_3 + B_2O_3 + 4NH_4H_2PO_4$

$GdBP_2O_8$ was prepared from 1:1:4 molar mixture of gadalinium oxide, boron oxide and diamonium hydrogen phosphate according to the reaction:

$$Gd_2O_3(s) + B_2O_3(s) + 4NH_4H_2PO_4(s) \rightarrow 2GdBP_2O_8(s) + 4NH_3(g) + 6H_2O(g)$$

This mixture was heated slowly in porcelain crucible at 600°C, 800°C, 900°C, 1000°C, 1100°C and 1200°C for 7 hours. After each heating, grinding was done.

2.3.2.3. Solid-State Reaction of $Dy_2O_3 + B_2O_3 + 4NH_4H_2PO_4$

The reaction mixture was prepared by weighing the stoichiometric amounts of reactants separately and grinding together in an agate mortar, then heating at 600°C, 800°C, 900°C, 1000°C, 1100°C and 1200°C for 7 hours. The expected reaction was:

$$Dy_2O_3(s) + B_2O_3(s) + 4NH_4H_2PO_4(s) \rightarrow 2DyBP_2O_8(s) + 4NH_3(g) + 6H_2O(g)$$

2.3.2.4.Solid-State Reaction of $Er_2O_3 + B_2O_3 + 4NH_4H_2PO_4$

The reactants were weighed separately and ground together in an agate mortar. Then the mixture were heated at different temperatures in the range of 600-1200°C in porcelain crucible. The following reaction was expected:

$$Er_2O_3(s) + B_2O_3(s) + 4NH_4H_2PO_4(s) \rightarrow 2ErBP_2O_8(s) + 4NH_3(g) + 6H_2O(g)$$

2.3.2.5.Solid-State Reaction of $Yb_2O_3 + B_2O_3 + 4NH_4H_2PO_4$

The reactants were mixed in the required proportions and crushed well in an agate mortar the mixture was heated at 600°C, 800°C, 900°C, 1000°C, 1100°C and 1200°C for 7 hours. The expected reaction was:

$$Yb_2O_3(s) + B_2O_3(s) + 4NH_4H_2PO_4(s) \rightarrow 2YbBP_2O_8(s) + 4NH_3(g) + 6H_2O(g)$$

CHAPTER III

RESULTS AND DISCUSSION

3.1. Solution Reactions for the Synthesis of Some New Rare Earth Diphosphates

3.1.1. Solution Reaction of $NdCl_3 + Na_4P_2O_7$

The solution of $NdCl_3$ which was obtained from the dissolution of Nd_2O_3 in dilute HCl solution, was treated with $Na_4P_2O_7$ solution. The violet gelatinous precipitate was filtered and dried in air.

The following reaction was predicted to take place in solution reaction of $NdCl_3$ with $Na_4P_2O_7$.

$$NdCl_3(aq) + Na_4P_2O_7(aq) \rightarrow NaNdP_2O_7.xH_2O(s) + 3Na^+(aq) + 3Cl^-(aq)$$

3.1.1.1. Thermal Study of $NaNdP_2O_7.4.5H_2O$ by TG-DTG and DSC Curves

Figure 3.1 shows the TG-DTG thermogram of hydrated $NaNdP_2O_7$ from room temperature up to 900°C.

In the TG curve, the weight loss can be divided into three stages. The TG weight loss in the first stage (14.23%) due to the elimination of 3.5 water molecules, according to the scheme:

$$NaNdP_2O_7.4.5H_2O \rightarrow NaNdP_2O_7.H_2O + 3.5H_2O$$

is close to the calculated value 15.58%. It is related to the endothermic peak at 103.7°C.

The second 1.74% and third weight loss 3.28% related to the endothermic peak observed at 270.8°C, are compatible with theoretical loss of one water molecule

(5.02%), which correspond to the formation of an amorphous anhydrous form of $NaNdP_2O_7$. The total weight loss is then 19.25% ($4.5H_2O$). This is in good agreement with the theoretical loss of 4.5 moles of H_2O from the obtained product (19.18%).

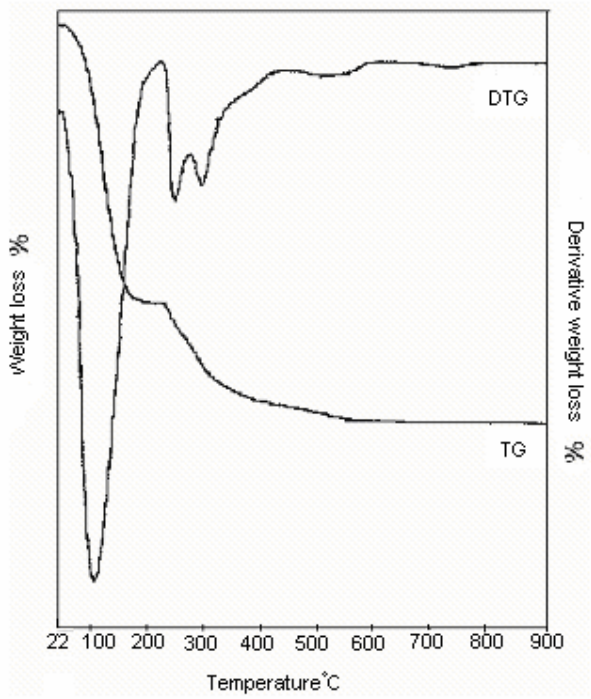

Figure 3.1. *TG-DTG curve of $NaNdP_2O_7.4.5H_2O$*

DSC study of compound indicated two endothermic peaks around 104 and 271^oC which are due to the elimination of water molecules from the hydrated sodium neodymium diphosphate (Fig.3.2).

The exothermic peak in the range 160-210^oC, with maximum rate observed at 175^oC is due to the formation of amorphous phase corresponding to the scheme:

$$NaNdP_2O_7.4.5H_2O \rightarrow NaNdP_2O_7.H_2O(amorphous) + 3.5H_2O$$

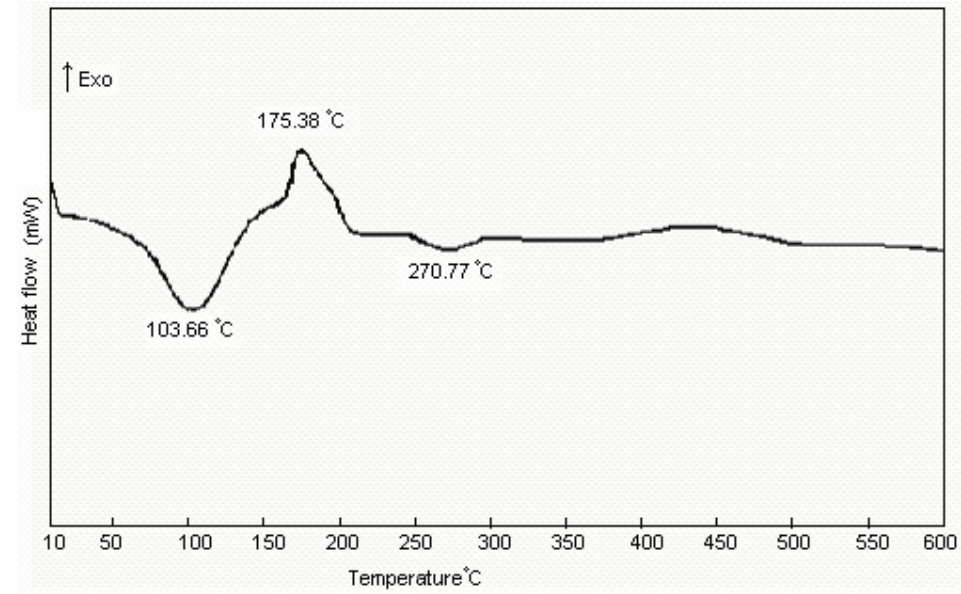

Figure 3.2. *DSC curve of* $NaNdP_2O_7.4.5H_2O$

The calculated enthalpy, ΔH for these two stages of the dehydration and for the phase transition of the title compound are summarized in Table 3.1.

Table 3.1. *Enthalpy (ΔH) for dehydration and for phase transition of* $NaNdP_2O_7.4.5H_2O$

Peaks	**T_i(^{o}C)**	**T_f(^{o}C)**	**T_m(^{o}C)**	**ΔH(J/g)**
1.Endo.	61	160	104	208.408
2.Exo.	163	205	175	-63.659
3.Endo.	246	289	271	14.290

Endo: *Endothermic;* ***Exo:*** *Exothermic.*

T_i: *initial temperature;* ***T_f:*** *final temperature;* ***T_m:*** *temperature with maximum rate.*

3.1.1.2. X-Ray Powder Diffraction Study of $NaNdP_2O_7.4.5H_2O$

The x-ray powder diffraction pattern (Fig.3.3.) of the product obtained from the solution reaction of $NdCl_3$ with $Na_4P_2O_7$ was amorphous. Then, to obtain crystalline

compound, this product was further dried in vacuum at 130°C and 270°C. These temperatures were decided depending on thermal analysis. But its XRD patterns of the products at these temperature were found again as amorphous.

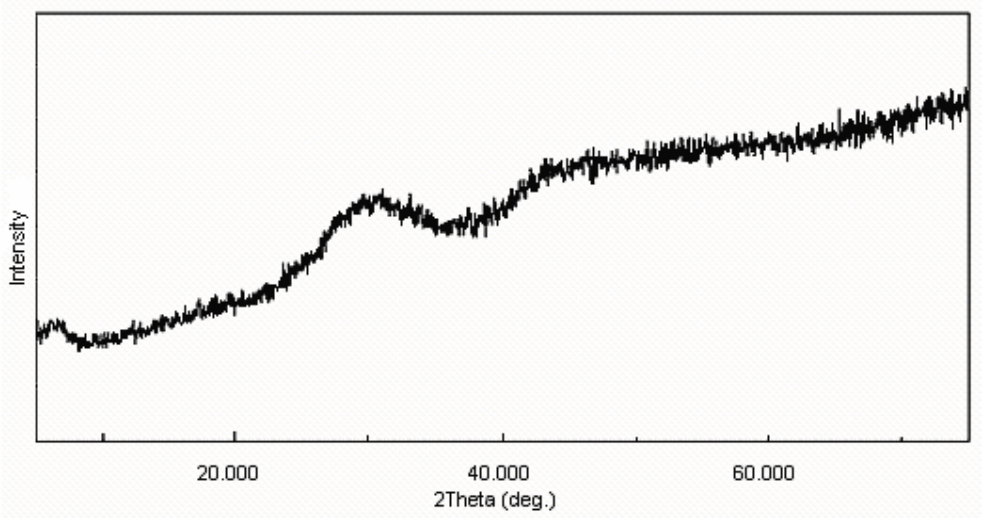

Figure 3.3. *X-Ray Powder Diffraction pattern of $NaNdP_2O_7.4.5H_2O$*

In an effort to isolate an anhydrous crystalline compound, the obtained product dried in vacuum was heated at 650, 700 and 750°C.

Examination of the X-ray powder data of the Nd compound prepared at 650°C, showed that the product was essentially a single phase. Some diffraction lines of $NdPO_4$ and $NaPO_3$ seemed to be present in the X-ray pattern, but their intensities were not consistent with the reported data. The powder data given in Figure 3.4 and table 3.2, were similar to those of $NaGdP_2O_7$ [10]. Therefore it was predicted that the primary phase was $NaNdP_2O_7$. It was indexed in the orthorhombic system and the refined lattice parameters were found to be a=12.579(7), b=15.10(l), c=16.03(1)Å (Table 3.2) which were in good agreement with the unit cell parameters of $NaGdP_2O_7$, so the two compounds were proved to be isostructural. The X-ray

powder diffraction studies at 700°C indicated that the product was still $NaNdP_2O_7$ with the same X-ray data which was obtained at 650°C. When the experiment was performed at 750°C, the product, $NaNdP_2O_7$, started to decompose into $NdPO_4$ and $NaPO_3$. But since $NaPO_3$ melts at this temperature and became amorphous, its diffraction lines did not appear in the X-ray pattern. Only $NaNdP_2O_7$ and $NdPO_4$ lines were observed in the X-ray data at 750°C.

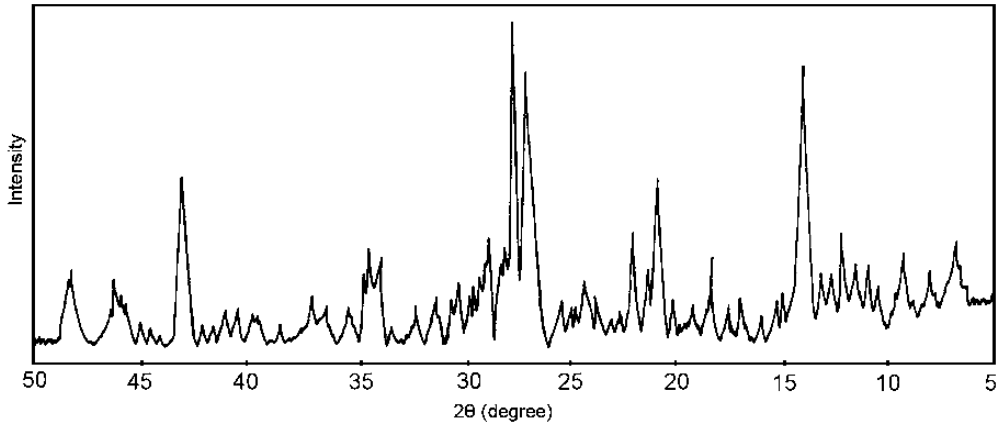

Figure 3.4. *X-Ray Powder Diffraction pattern of $NaNdP_2O_7$*

Table 3.2 *X-ray powder diffraction data of $NaNdP_2O_7$. Orthorhombic: a=12.579(7), b=15.10(1), c=16.03(1)Å., Rad. CuK_α*

I/I_o	d_{obs}	d_{calc}	hkl
26	12.54	12.56	100
21	10.94	10.98	011
29	9.57	9.65	110
11	8.28	8.27	111
27	8.07	8.00	002
22	7.60	7.55	020
34	7.25	7.07	012
21	6.90	6.82	021
21	6.56	6.47	120
88	6.28	6.28	200

18	5.86	5.84	201
13	5.79	5.80	210
13	5.54	5.49	022
20	5.24	5.33	003
20	5.02	5.03	030
32	4.84	4.83	220
15*	4.67	4.67	130
18	4.37	4.36	023
69	4.24	4.26	032
21	4.162	4.152	222
12*	4.114	4.115	123
39*	4.035	4.033	310
12	3.927	3.925	213
14	3.895	3.910	311
11	3.831	3.812	231
14	3.754	3.772	040
24	3.663	3.660	320
11	3.596	3.579	223
12	3.541	3.524	141
14	3.500	3.513	133
87	3.280	3.293	142
100	3.198	3.201	005
53	3.157	3.154	331
42	3.132	3.131	034
45*	3.077	3.073	410
19*	3.039	3.038	134
18*	3.028	3.018	050
13	2.991	2.985	332
14	2.957	2.947	025
26*	2.937	2.934	150
16	2.903	2.892	304
28*	2.831	2.824	052
18	2.763	2.755	152
11	2.667	2.663	430
46	2.625	2.627	431

49	2.613	2.609	106
38*	2.579	2.571	153
20	2.520	2.511	500
20	2.455	2.448	350
26*	2.411	2.409	054
9*	2.348	2.341	352
16*	2.292	2.295	344
18	2.284	2.283	522
26	2.239	2.238	163
25	2.202	2.196	055
13	2.173	2.175	450
13*	2.156	2.148	425
72*	2.098	2.092	600
7*	2.0659	2.0662	444
12	2.0324	2.0326	406
15	2.0123	2.0007	612
17	1.9893	1.9832	018
41	1.9636	1.9626	460
19	1.9529	1.9480	461
44	1.8861	1.8845	436
38	1.8787	1.8764	552

* Matching $NdPO_4$ lines

3.1.1.3. Infrared Spectroscopy Studies of the Heated Products of $NaNdP_2O_7.4.5H_2O$ at Different Temperatures.

The IR spectra of a number of diphosphate sa1ts have been examined in literature [75–80] and it has been found that their strong characteristic absorption bands appeared in the region of 950–910 and 670–735 cm^{-1}. $C_{2\upsilon}$ symmetry and a bent bridge eclipsed orientation of the two PO_3 groups through P-O-P bridge of the $P_2O_7^{4-}$ ion was supported by Palmer [78].

The number of normal modes of vibrations is 21, but only 17 are IR

active [81]. The number of vibrational modes could be increased by both the appearence of combinations and overtones.

On the other hand, the IR and Raman spectra of monoclinic α- and β- $Mg_2P_2P_7$, and α-$Ca_2P_2O_7$ orthorhombic α- $Sr_2P_2O_7$ and α- $Ba_2P_2O_7$ and triclinic $Ca_2P_2O_7$ were predicted using the $C_{2\upsilon}$ free ion group symmetry species [82–84].

Recently, the infrared and Raman spectra of orthorhombic $NaGdP_2O_7$ were interpreted by Kızılyallı et al.[9]. They assigned the vibrational bands for $NaGd_2P_2O_7$ on the basis of Cornilsen's discussions on $Ca_2P_2O_7$, $Mg_2P_2O_7$ and $Sr_2P_2O_7$ [83] and Walrafen's calculations [85] for the $C_{2\upsilon}$ free ion group symmetry. Later on the vibrational spectra of $M^{I}LnP_2O_7$ (M^{I}=Rb, Cs; Ln=rare earth) have been studied using factor group analysis [14, 86].

In this work, the infrared spectra of the products formed upon heating of $NaNdP_2O_7$ at different temperatures are illustrated in Figure 3.5–3.6.

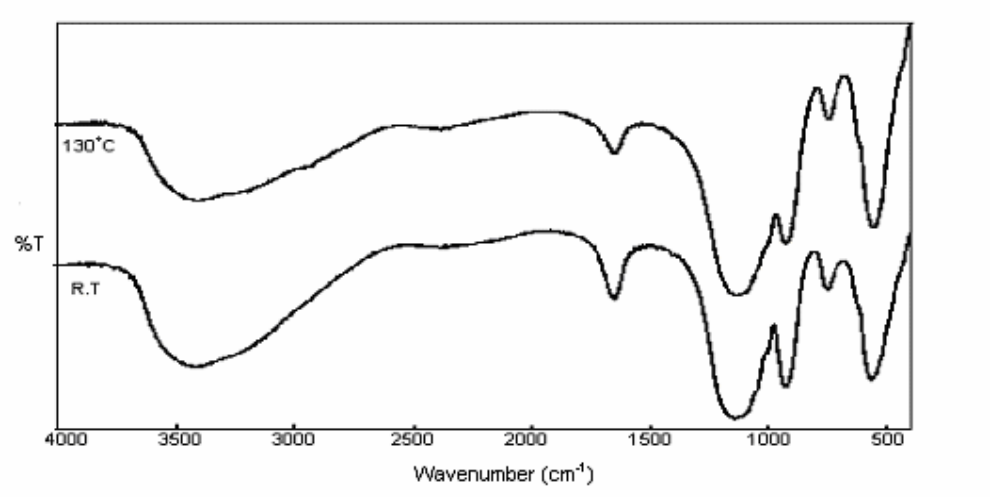

Figure 3.5 *The infrared spectra of $NaNdP_2O_7.4.5H_2O$ at room temperature and 130^oC*

According to the infrared spectra of $NaNdP_2O_7.4.5H_2O$ and its heated products, this compound is stable in the range 25-61^oC.

With the help of the TG-DTG and DSC study of $NaNdP_2O_7.4.5H_2O$, we can suggest that infrared spectra of the products at 650-750^oC indicate a great change, compared to the initial one. Differences are characterized by decreases of the number of the water bands (υH_2O and δH_2O) and some bands location, they correspond to the removal of all water molecules, broadened bands appear in the infrared spectra after heating the initial product at 650^oC indicating the formation of crystalline phase of $NaNdP_2O_7$.

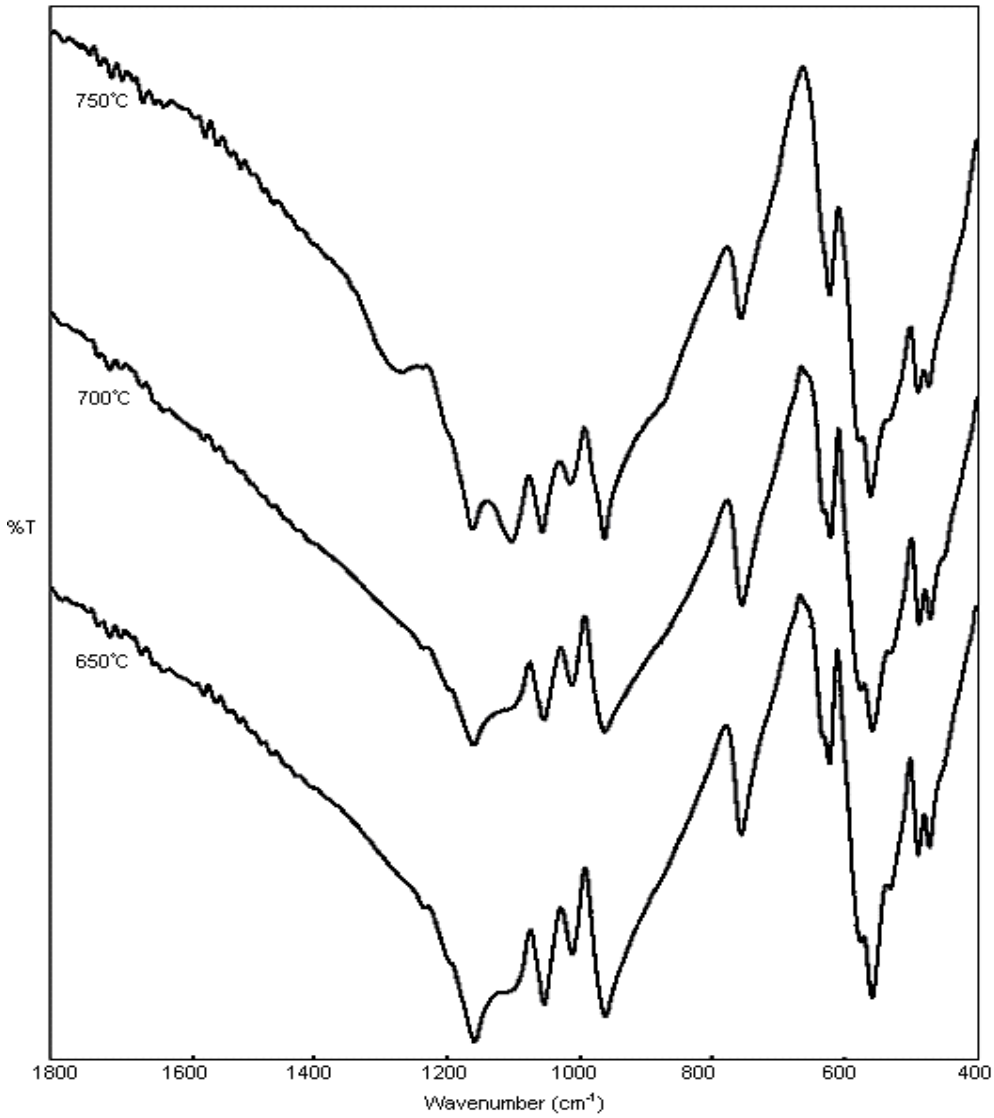

Figure 3.6 *IR spectra of the heated products of $NaNdP_2O_7.4.5H_2O$ at different temperatures.*

The infrared spectrum of the product obtained at 650°C and predicted to be $NaNdP_2O_7$ was found to be isostructural with $NaGdP_2O_7$ [10]. Examination of the IR data (Fig.3.6), indicated that there was a good agreement with the reported values for $NaGdP_2O_7$ [10].

3.1.2.Solution Reaction of $GdCl_3 + Na_4P_2O_7$

The following reaction was expected to take place in solution reaction of $GdCl_3$ with $Na_4P_2O_7$.

$$GdCl_3(aq) + Na_4P_2O_7(aq) \rightarrow NaGdP_2O_7.xH_2O(s) + 3Na^+(aq) + 3Cl^-(aq)$$

3.1.2.1.Thermal Study of $NaGdP_2O_7.4H_2O$ by TG-DTG and DSC Curves

From room temperature up to 900°C, Figure 3.7 indicates the TG-DTG thermogram of $NaGdP_2O_7.4H_2O$.

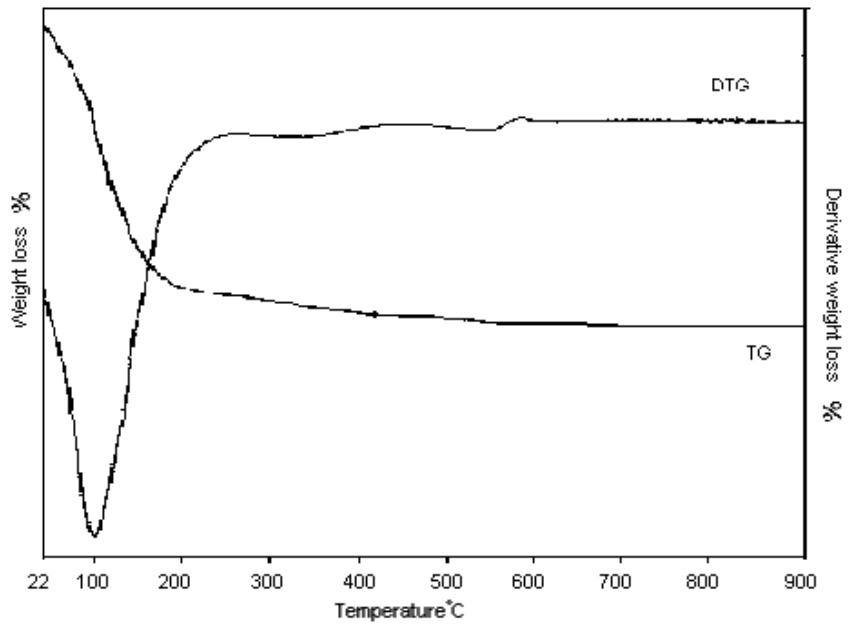

Figure 3.7 *TG-DTG curve of $NaGdP_2O_7.4H_2O$*

In the thermogravimetric analysis of $NaGdP_2O_7.4H_2O$ the total weight loss was found as 17.53% in one stage. This is in good agreement with the calculated weight

loss 16.89% of 4 moles of H_2O from the product. The elimination of water molecules from $NaGdP_2O_7.4H_2O$ can be explained by the following reaction:

$$NaGdP_2O_7.4H_2O \rightarrow NaGdP_2O_7 + 4H_2O$$

Figure 3.8 shows the DSC thermogram of $NaGdP_2O_7.4H_2O$. In the differential scanning calorimetric analysis of sodium gadolinium diphosphate tetrahydrate, one endotherm and one exotherm were observed at 100.62°C and 545.45°C respectively. The endothermic curve at 100.62°C is considered to result from the elimination of 4 water molecules from the structure of $NaGdP_2O_7.4H_2O$. In the range 535-555°C, the DSC curve exhibits an exothermic peak at 545.45°C which is accompained by the decomposition of the title compound to $GdPO_4$ [87], $HGdP_2O_7$ [2] and $Gd_4(P_2O_7)_3$ [88].

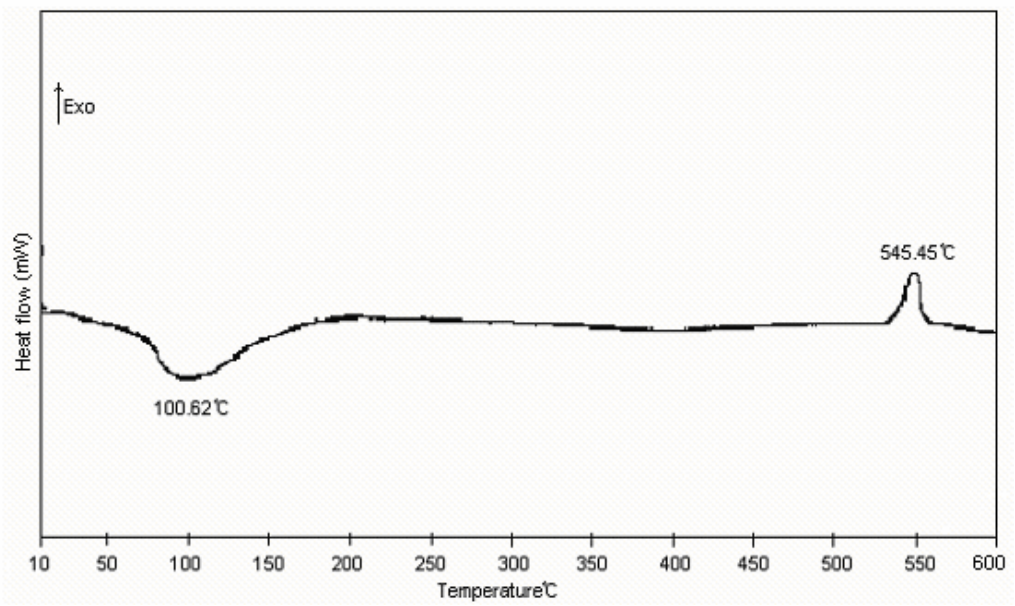

***Figure 3.8**-DSC curve of $NaGdP_2O_7.4H_2O$*

The calculated enthalpy, ΔH of these two DSC curves are given in Table 3.3.

Table 3.3. *Enthalpy,(ΔH) for dehydration and for phase transition of* $NaGdP_2O_7.4H_2O$

Peaks	T_i(°C)	T_f(°C)	T_m(°C)	ΔH(J/g)
1.Endo.	65	210	100	253.688
2.Exo.	537	554	545	-39.534

Endo:*Endothermic;* ***Exo:****Exothermic.*

T_i***:*** *initial temperature;* T_f***:*** *final temperature;* T_m***:*** *temperature with maximum rate.*

3.1.2.2. X-Ray Powder Diffraction Study of $NaGdP_2O_7.4H_2O$

The solution of $GdCl_3$ which was obtained from the dissolution of Gd_2O_3 in dilute HCl solution, was treated with $Na_4P_2O_7$ solution. The white gelatinous precipitate was filtered and dried in air. The X-ray powder diffraction pattern (Fig.3.9.) of this product was amorphous. Then, to obtain crystalline compound, this product was further dried in vacuum at 130°C. This temperature was decided depending on thermal analysis. But its XRD pattern at this temperature was found again as amorphous.

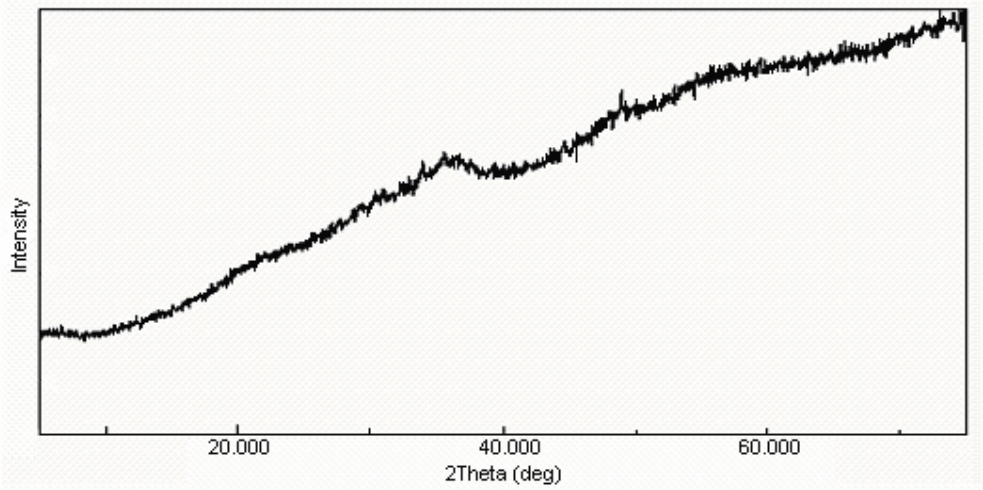

Figure 3.9. *XRD data for* $NaGdP_2O_7.4H_2O$

In an effort to isolate an anhydrous crystalline compound, the obtained product dried in vacuum was heated at 550, 650 and 750^{o}C.

By investigating XRD data of Gd compound heated at 650, 700 and 750^{o}C, the diffraction lines belonging to $GdPO_4$ [87], $HGdP_2O_7$ [2] and $Gd_4(P_2O_7)_3$ [88] compounds appeared. When the compound obtained at 750°C was reheated at 900°C, $Gd_2P_4O_{13}$ was observed as a product which was previously reported [73,90].

3.1.2.3. Infrared Spectroscopy Studies of the Heated Products of $NaGdP_2O_7.4H_2O$ at Different Temperatures.

The IR spectra of the products obtained from the solution reaction of $GdCl_3$ with $Na_4P_2O_7$ is given in Figure 3.10.

In the IR spectra of $NaGdP_2O_7.4H_2O$ at room temperature and 130^{o}C, common features are the bands due to the symmetric and asymmetric vibrations of the POP bridge (υ_s POP and υ_{as} POP) observed in the range 700-950 cm^{-1}[86] which indicate the presence of the $(P_2O_7)^{4-}$ anions with a bent POP angles in this compound.

With the help of the TG-DSC study of the title compound, we can suggest that infrared spectra established in the range 25-130^{o}C can be attributed to the $NaGdP_2O_7.4H_2O$.

In the IR region between 2800cm^{-1}-3800cm^{-1}, the broad bands correspond to the streching vibration of water molecules (υ_{H2O}) [80]. The bending vibrations of H_2O (δ_{H2O}) are seen in the range 1600–1700 cm^{-1} [91-92].

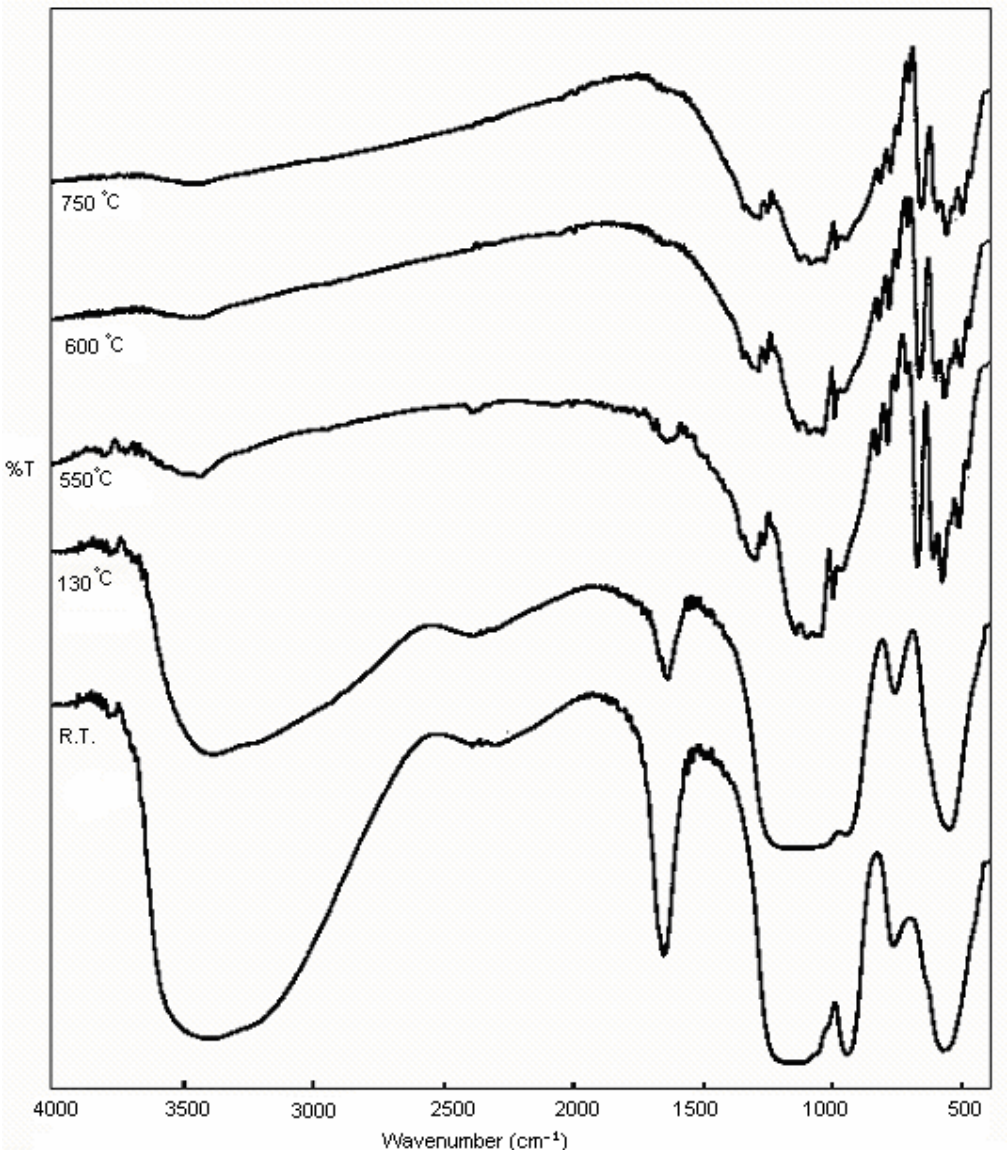

Figure 3.10. *IR spectra of the $NaGdP_2O_7.4H_2O$ at different temperatures.*

3.1.3. Solution Reaction of $DyCl_3$ + $Na_4P_2O_7$

The following reaction was expected to take place in solution reaction of $DyCl_3$ with $Na_4P_2O_7$.

$$DyCl_3(aq) + Na_4P_2O_7(aq) \rightarrow NaDyP_2O_7.xH_2O(s) + 3Na^+(aq) + 3Cl^-(aq)$$

3.1.3.1. Thermal Study of $NaDyP_2O_7.5H_2O$ by TG-DTG and DSC Curves

From room temperature up to 900 on 600°C, Figure 3.11 shows the TG-DTG thermogram of $NaDyP_2O_7.5H_2O$. In the TG curve, the weight loss 20.49% is corresponding to the elimination of 5 water molecules in one stage, due to the scheme:

$$NaDyP_2O_7.5H_2O \rightarrow NaDyP_2O_7 + 5H_2O$$

It is close to the calculated value 20.02%.

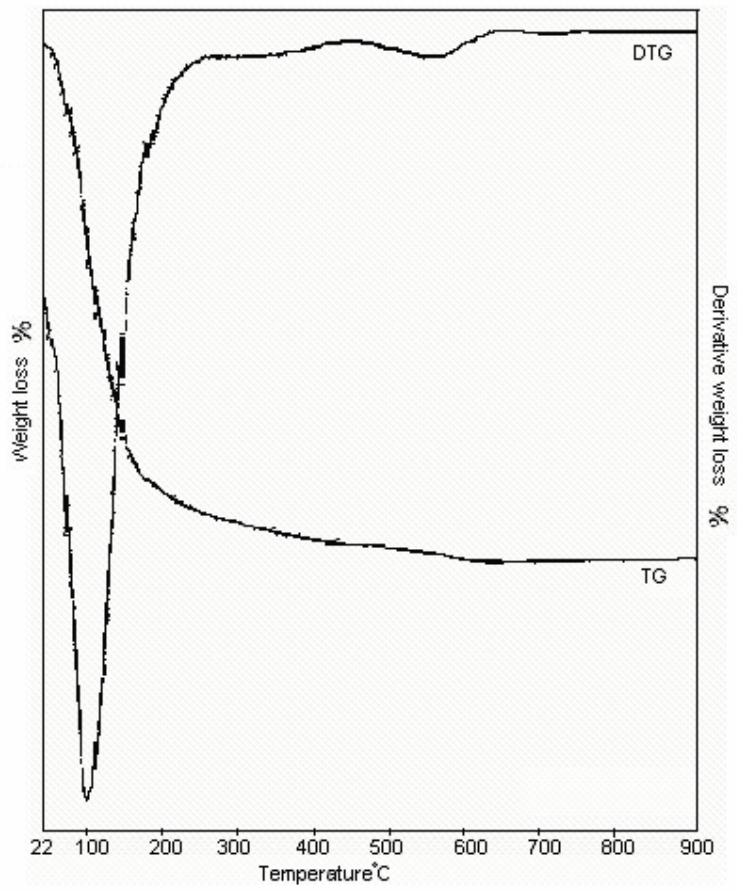

Figure 3.11. *TG-DTG Curves of $NaDyP_2O_7.5H_2O$.*

Figure 3.12 indicates the differential scanning calorimeter of Dy compound. In the range 50-200°C, one observed endotherm in the DSC curve at 101°C is

considered to result from the removal of water molecules from the structure of $NaDyP_2O_7.5H_2O$.

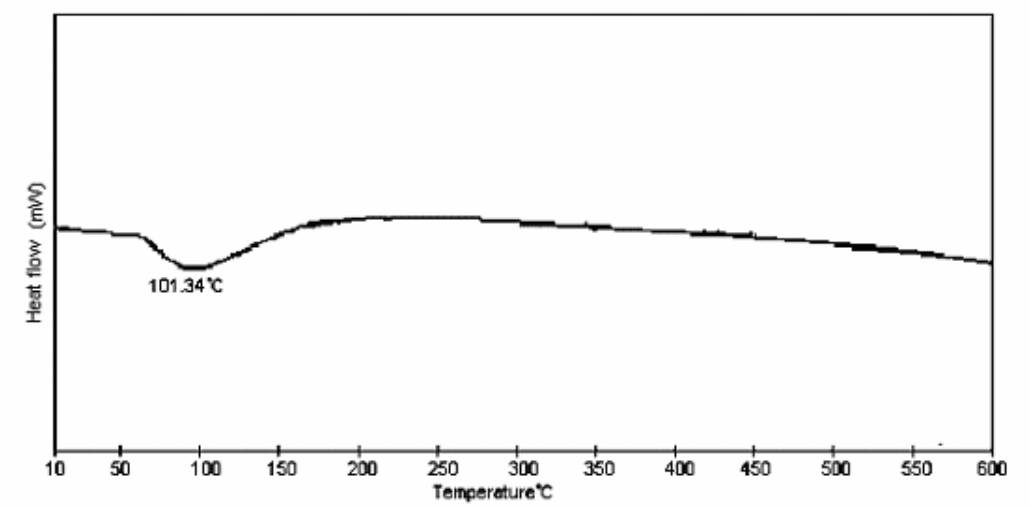

Figure 3.12. *DSC Curve of $NaDyP_2O_7.5H_2O$*

The calculated enthalpy, ΔH of the dehydration of 5 water molecules is summarized in Table 3.4.

Table 3.4. *Enthalpy, ΔH for dehydration of $NaDyP_2O_7.5H_2O$*

Peaks	**T_i(^{o}C)**	**T_f(^{o}C)**	**T_m(^{o}C)**	**ΔH(J/g)**
1.Endo.	65.52	165.08	101.34	245.866

Endo:*Endothermic.*

T_i: *initial temperature;* ***T_f:*** *final temperature;* ***T_m:*** *temperature with maximum rate.*

3.1.3.2. X-Ray Powder Diffraction Study of $NaDyP_2O_7.5H_2O$

When the solution of $DyCl_3$ was treated with $Na_4P_2O_7$ solution, the gelatinous white product was obtained. The XRD pattern (Figure 3.13) of this product was found as amorphous.

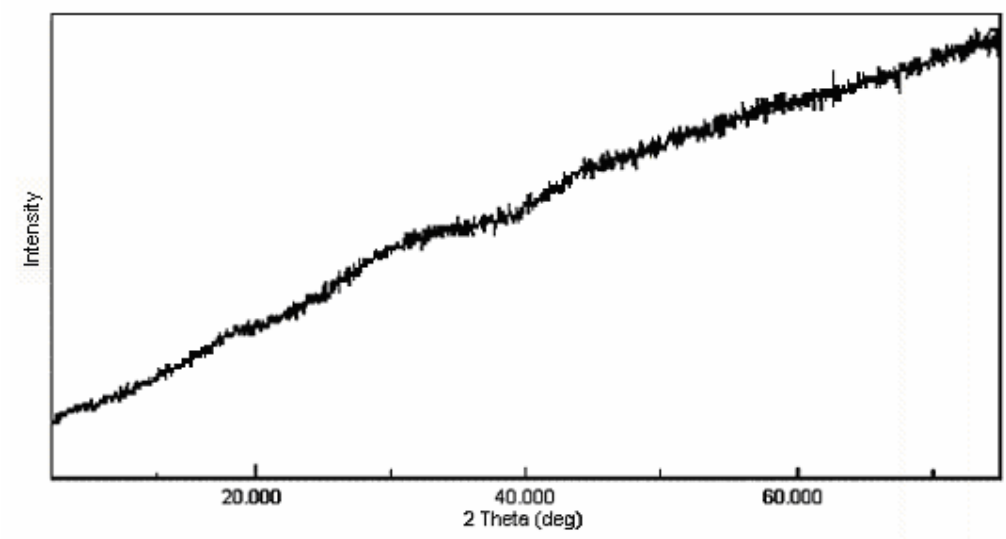

Figure 3.13. *XRD patern of $NaDyP_2O_7.5H_2O$*

Therefore, it was further heated at 150^{o}C, but the crystalline form of this product was not obtained. Then, further heating was done at 540^{o}C to get the anhydrous crystalline diphosphate compound by removing water molecules. When the XRD pattern (Figure 3.14) of the obtained product was examined, the result was again amorphous.

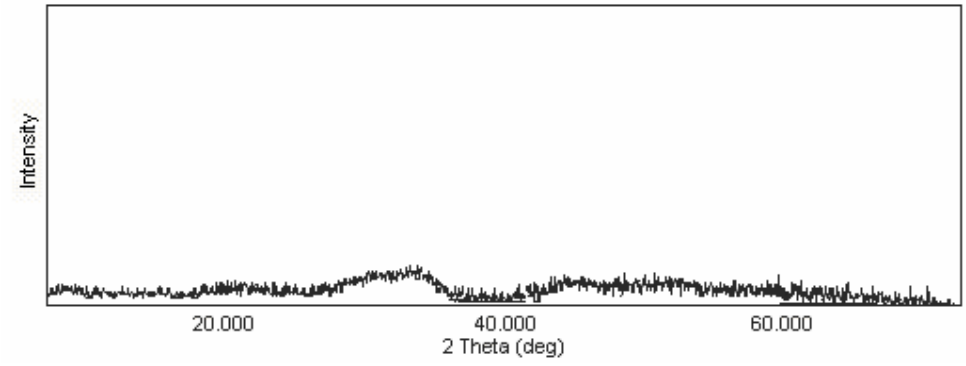

Figure 3.14 *XRD patern of the obtained product at 540^{o}C*

To reach the crystallinity of this diphosphate salt further heating was done at 650^{o}C. In the examination of the XRD pattern of this compound, it was seen that all d-lines observed were overlapping those of the tetragonal $DyPO_4$ (see JCPDS card No:26-593); no extra diffraction peak from other phases occured. It means that the crystal lattice of $NaDyP_2O_7$ should possess the same lattice as that of $DyPO_4$ [74] and introducing extra Na, P and O atoms simultaneously into $DyPO_4$ lattice adds no extra reflection [89].

It was found that the alkali rare earth diphosphates with the formula $M^{I}LnP_2O_7$ possess several types of structure, some crystallizing into the lattice of ortophosphates called pseudo-diphosphates, others being real diphosphates.

For the pseudo-diphosphates, the lattices were considered isostructural with those of the corresponding $LnPO_4$, with similar XRD patterns and vibrations [13].

In this part of this work, we decided that the prepared compound was pseudo-diphosphate, $NaDyP_2O_7$, as reported by Shao-Long Tie [13]. Its structure, possessing the tetragonal $DyPO_4$ lattice and filling the channels with chain $NaPO_3$ was characterized by its XRD pattern.

3.1.3.3. Infrared Spectroscopy Studies of $NaDyP_2O_7.5H_2O$ at Different Temperatures

The IR spectra of the products obtained in this part of this work are given in Figure 3.15.

At low temperatures, the similar vibrational bands related with $P_2O_7^{4-}$ anion observed for the other $NaLnP_2O_7.xH_2O$ (Ln: Nd, Gd) compounds in the previous sections were obtained as seen in Figure 3.15.

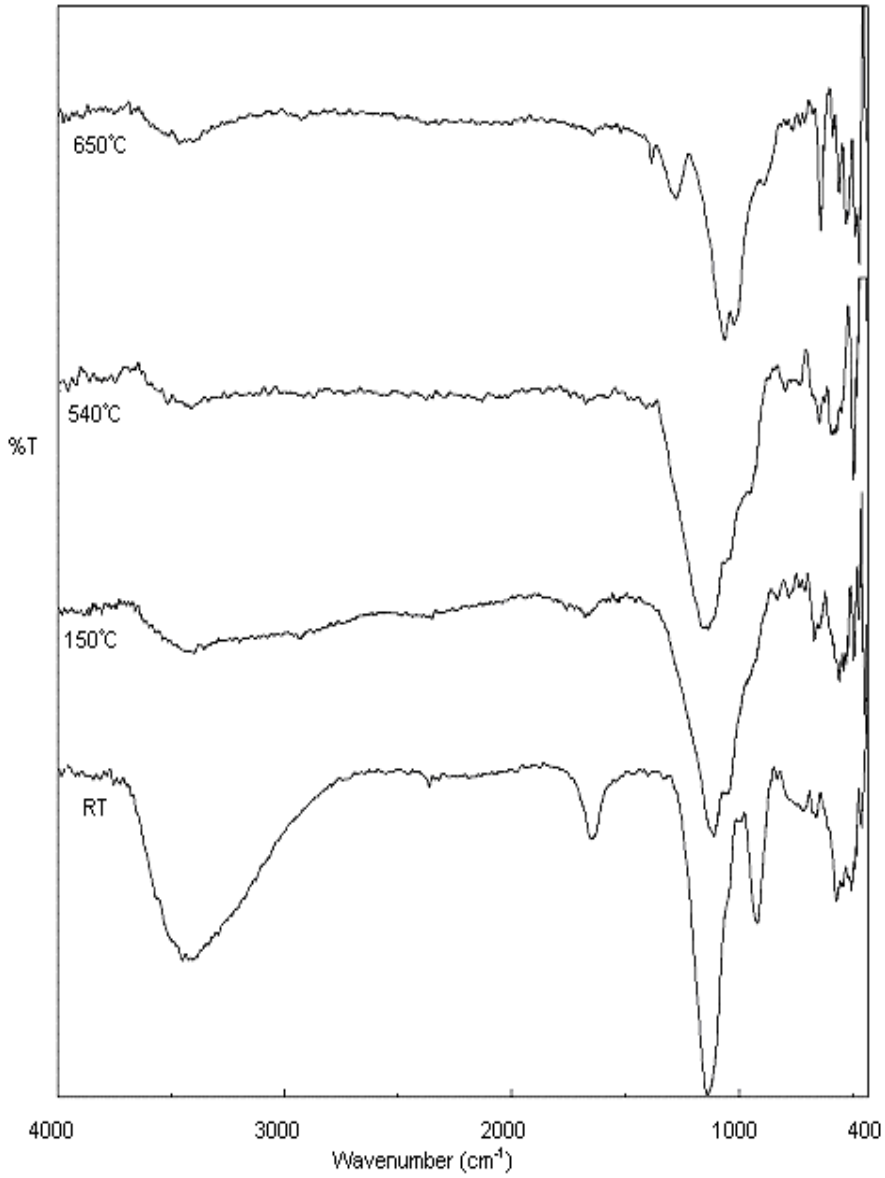

Figure 3.15. *IR spectra of $NaDyP_2O_7.5H_2O$ at different temperatures*

The vibrations and corresponding assignments for pseudo-diphosphate $NaDyP_2O_7$, are summarized in Table 3.5. For comparison, results for $DyPO_4$ are also quoted.

Table 3.5. *Infrared Vibrations of* $NaDyP_2O_7$ *and tetragonal* $DyPO_4$ (in cm^{-1})

$NaDyP_2O_7$	$DyPO_4$	Assignment
1275	-	PO_3, υ_{as} (P-O)
1064	1053	PO_4, υ_{as} (P-O)
1018	1020	PO_4, υ_{as} (P-O)
890	-	PO_3, υ_{as} (P-O-P)
764 sh	-	PO_3, υ_s (P-O-P)
713 sh	-	PO_3, υ_s (P-O-P)
640	635	PO_4, δ_{as} (O-P-O)
559	-	PO_4, δ_{as} (O-P-O)
523	524	PO_4, δ_{as} (O-P-O)
470	-	PO_4, δ_s (O-P-O)

3.1.4. Solution Reaction of $ErCl_3 + Na_4P_2O_7$

The expected equation through the solution reaction of $ErCl_3$ with $Na_4P_2O_7$ is as follows:

$ErCl_3$ (aq) + $Na_4P_2O_7$ (aq) → $NaErP_2O_7.xH_2O$ (s) + $3Na^+$ (aq) + $3Cl^-$ (aq)

3.1.4.1 Thermal Study of $NaErP_2O_7.xH_2O$ by DSC Curve

Figure 3.16 shows the DSC thermogram of $NaErP_2O_7.xH_2O$ from room temperature up to 600 ^oC.

In the DSC curve , only one endothermic peak was observed in the range 25-200 ^oC, at 98,67 ^oC is considered to result from the removal of water molecules from the structure of $NaErP_2O_7.xH_2O$. However, we could not determine the amount of the removal of water because of the lack of thermogravimetric analysis.

Therefore, the elimination of x water molecules can be shown in one stage, due to the scheme;

$$NaErP_2O_7.xH_2O(s) \rightarrow NaErP_2O_7(s) + xH_2O(g)$$

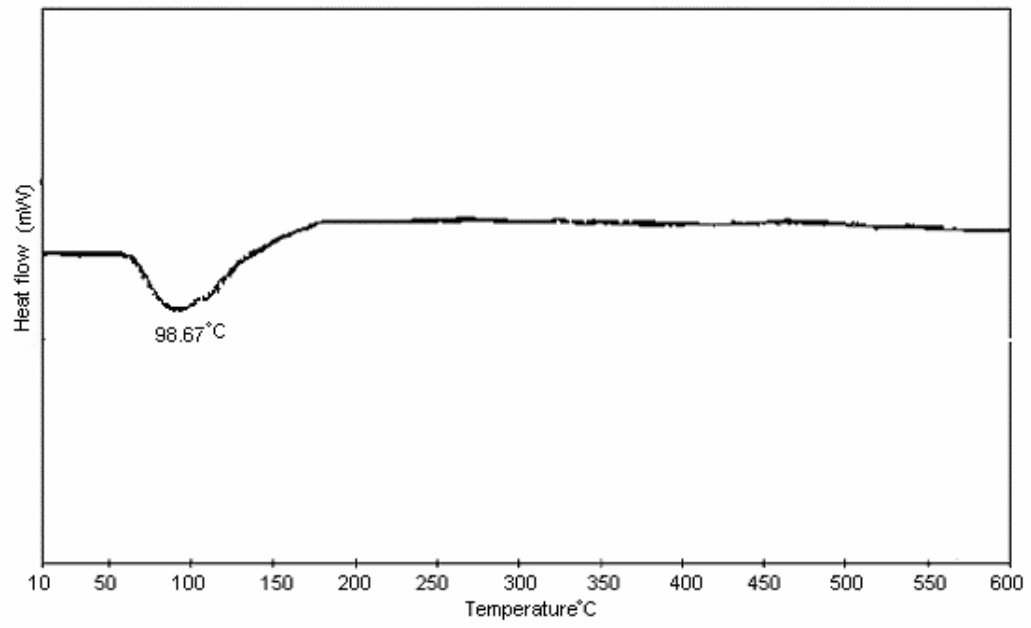

Figure 3.16. *DSC Curve of the $NaErP_2O_7.xH_2O$*

The calculated enthalpy, ΔH of the dehydration of x water molecules is summarized in Table 3.6.

Table.3.6 . *Enthalpy, ΔH for dehydration of $NaErP_2O_7.xH_2O$*

Peaks	**T_i(°C)**	**T_f(°C)**	**T_m(°C)**	**ΔH(J/g)**
endo	62.71	146.31	98.67	330.240

Endo: *Endothermic.*

T_i: *initial temperature;* ***T_f:*** *final temperature;* ***T_m:*** *temperature with maximum rate.*

3.1.4.2. XRD Study of $NaErP_2O_7.xH_2O$

By the treatment of the solution of $ErCl_3$ with $Na_4P_2O_7$ solution, the gelatinous pink product was obtained. The XRD pattern (Figure 3.17) of this product was found as amorphous. Thus, it was further heated at 150°C, but the crystalline form of this product was not obtained.

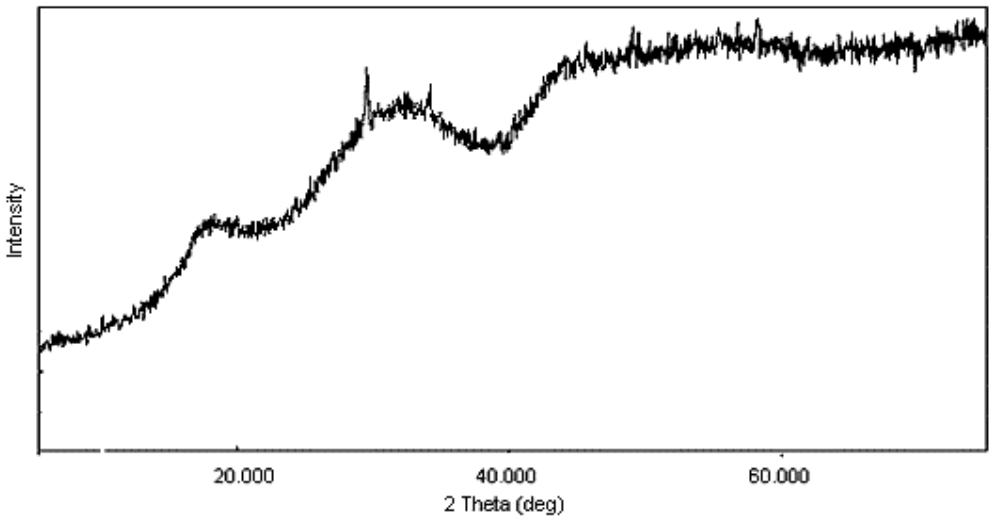

Figure.3.17 *XRD pattern of* $NaErP_2O_7.xH_2O$

To produce the anhydrous crystalline sodium erbium diphosphate compound, further heating was done at 550°C. When the XRD pattern (Figure 3.18) of the product obtained at 550°C was analyzed, it was found that its d-spacings overlapped those of the tetragonal $ErPO_4$ and no extra d-lines from other compounds occured as shown in Table 3.7. Therefore, it was suggested that, the structure of $NaErP_2O_7$ possessing the tetragonal $ErPO_4$ lattice and filling the channels with chain $NaPO_3$, was found as pseudo-diphosphate [13].

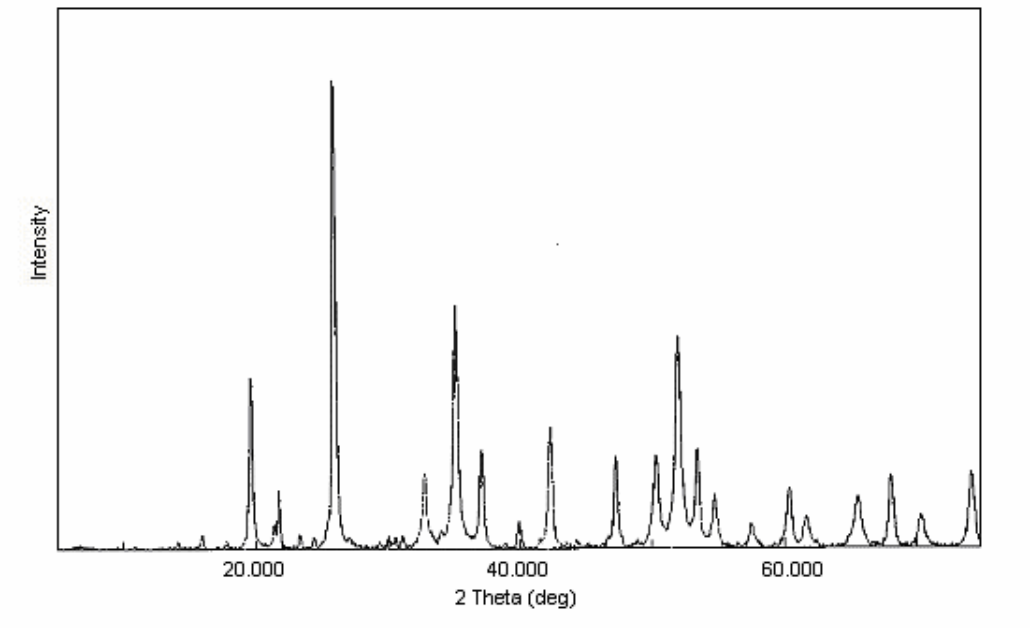

Figure 3.18. *X-Ray Powder Diffraction Pattern of $NaErP_2O_7.xH_2O$ at 550^oC.*

Table 3.7. *Comparison of the XRD data for $NaErP_2O_7$ and tetragonal $ErPO_4$ (J.C.P.D.S. Card No: 09-0383).*

I/I_o(this work)	**d-value(thiswork)**	**d-value($ErPO_4$)**
54	4.512	4.52
100	3.425	3.43
20	2.728	2.733
61	2.550	2.554
18	2.422	2.426
18	2.134	2.1382
11	1.919	1.9224
16	1.811	1.8144
42	1.756	1.7596
12	1.713	1.7157
7	1.674	1.6771
9	1.532	1.5347
11	1.422	1.4244
8	1.373	1.3792

3.1.4.3. IR Study of $NaErP_2O_7.xH_2O$

The IR spectra of the products obtained from the solution reaction of $ErCl_3$ with $Na_4P_2O_7$ is given in Figure 3.19.

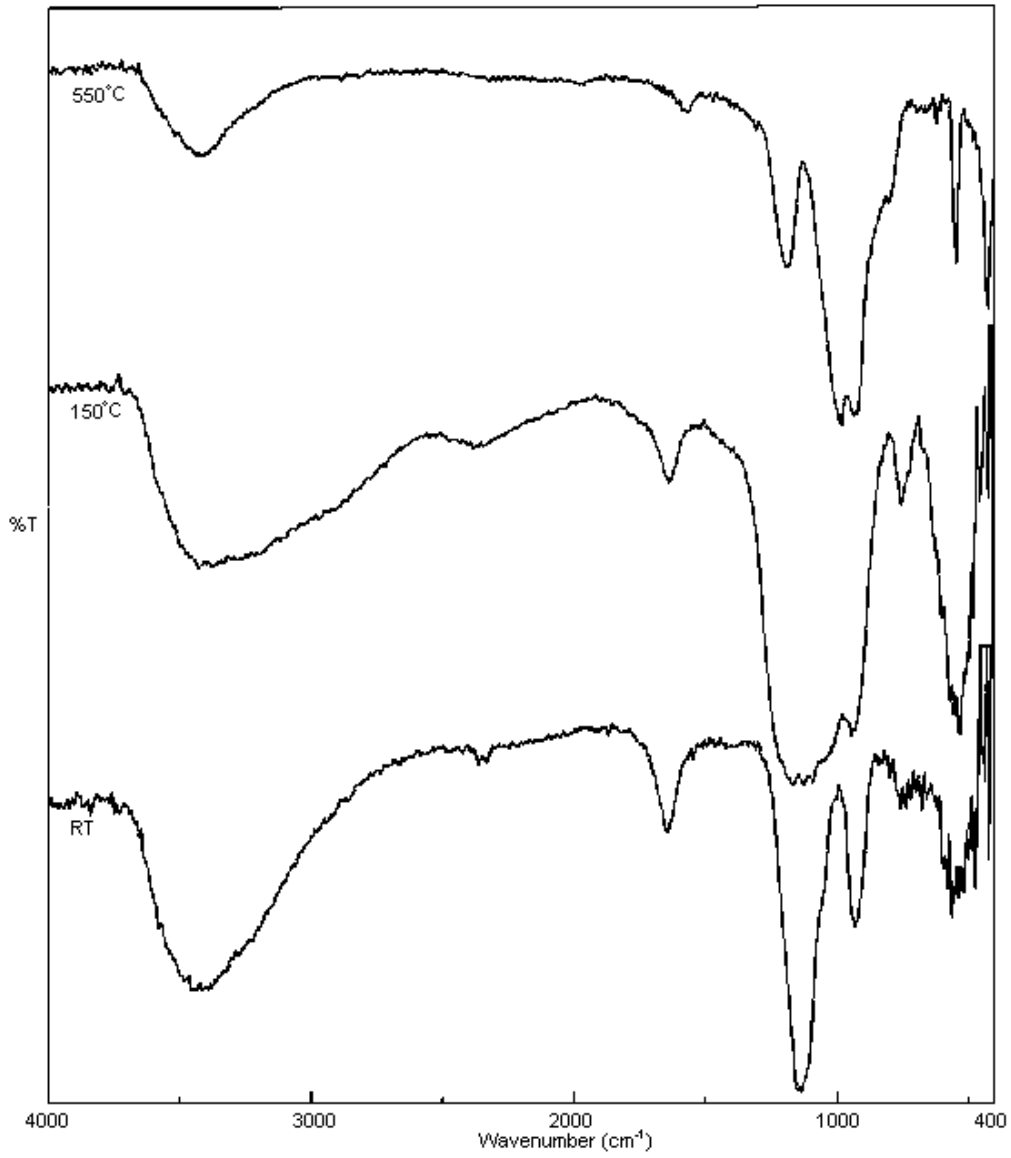

Figure 3.19 *IR spectra of the $NaErP_2O_7.xH_2O$ at different temperature.*

The vibrations and corresponding assignments for pseudo-diphosphate $NaErP_2O_7$ summarized in Table 3.8.

Table.3.8 *Infrared Vibrations of $NaErP_2O_7$ and Tetragonal $ErPO_4$ (in cm^{-1})*

$\upsilon_{(cm-1)}$ for $NaErP_2O_7$	$\upsilon_{(cm-1)}$ for $ErPO_4$	Assignments
1267	_	PO_3, υ_{as}(P-O)
1069	1058	PO_4, υ_{as}(P-O)
1017	1021	PO_4, υ_{as}(P-O)
884	_	PO_3, υ_{as}(P-O-P)
770	_	PO_3, υ_{s}(P-O-P)
714	_	PO_3, υ_{s}(P-O-P)
638	654	PO_4, δ_{as}(O-P-O)
520	525	PO_4, δ_{as}(O-P-O)

3.1.5. Solution Reaction of $YbCl_3 + Na_4P_2O_7$

The following reaction was predicted to take place in solution reaction of $YbCl_3$ with $Na_4P_2O_7$.

$$YbCl_3(aq) + Na_4P_2O_7(aq) \rightarrow NaYbP_2O_7.xH_2O(s) + 3Na^+(aq) + 3Cl^-(aq)$$

3.1.5.1. Thermal Study of $NaYbP_2O_7.xH_2O$

Figure 3.20 indicates the DSC thermogram of $NaYbP_2O_7.xH_2O$ from room temperature up to 600°C.

In the differential scanning calorimetric analysis, only one endotherm was observed at 107.85°C. This endothermic curve was considered to result from the elimination of x water molecule from the structure of $NaYbP_2O_7.xH_2O$. However, it was not possible to find the amount of water removed from the dehydrated diphosphate compound because of the lack of TG data.

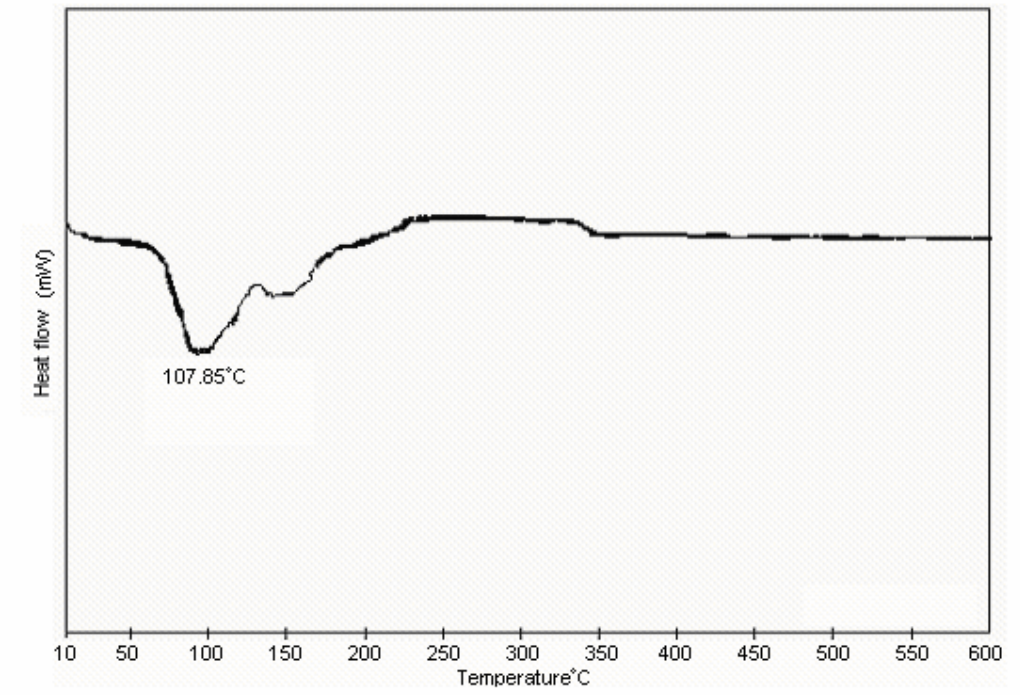

Figure 3.20. *DSC Curve of the $NaYbP_2O_7.xH_2O$*

The elimination of x mole of water occured in one stage, due to the scheme:

$$NaYbP_2O_7.xH_2O(s) \rightarrow NaYbP_2O_7(s) + xH_2O(g)$$

The calculated enthalpy, ΔH of the dehydration of x water molecule is summarized in Table 3.9.

Table.3.9. *Enthalpy, ΔH for dehydration of $NaYbP_2O_7.xH_2O$*

Peaks	**T_i(^{o}C)**	**T_f(^{o}C)**	**T_m(^{o}C)**	**ΔH(J/g)**
Endo.	72.87	122.89	107.85	442.857

Endo:*Endothermic.*

T_i: *initial temperature;* ***T_f:*** *final temperature;* ***T_m:*** *temperature with maximum rate.*

3.1.5.2. X-Ray Powder Diffraction Study of $NaYbP_2O_7.xH_2O$

The hydrated sodium ytterbium diphosphate was obtained as a fine white crystalline powder from the solution reaction of $YbCl_3$ with $Na_4P_2O_7$.

The X-ray powder diffraction pattern for this compound, given in Figure 3.21, contains a series of sharp reflections. But attemps to prepare crystals for single crystal X-ray structural analysis have been unsuccessful.

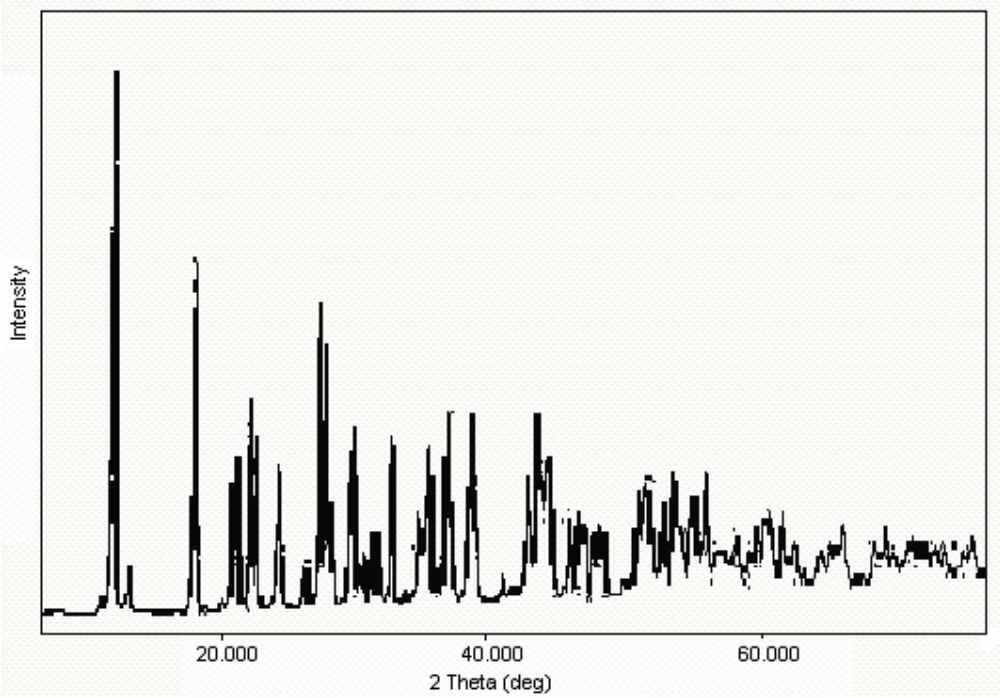

Figure 3.21. *XRD Pattern of $NaYbP_2O_7.xH_2O$.*

To obtain anhydrous, crystalline $NaYbP_2O_7$, the hydrated ytterbium compound was heated at 500 ^oC. XRD pattern (Figure 3.22) of this product showed the formation of a new crystalline compound by dehydration of some water molecules. The examination of the X-ray powder data, showed that this compound has been crystallized but we could not indexed the pattern because of the complex structure.

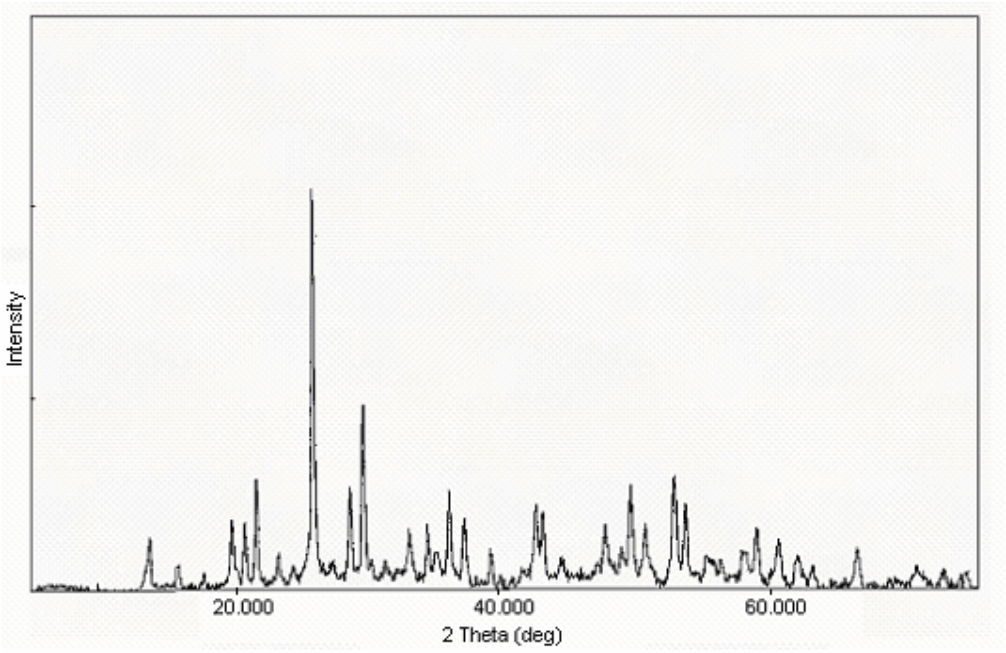

Figure 3.22. *XRD Pattern of $NaYbP_2O_7$.*

3.1.5.3. IR Study of of $NaYbP_2O_7.xH_2O$

Figure 3.23 presents the IR spectra of the hydrated and dehydrated ytterbium compound. When we analyze the IR spectrum of hydrated $NaYbP_2O_7.xH_2O$, the characteristic bands of crystallization water can be observed at 3412 and 1647 cm^{-1}. The strong absorption bands observed at 1154 and 1105 cm^{-1} can be attributed to the O-P-O stretching vibrations, whereas the vibrational bands at 942 and 749 cm^{-1} are assigned respectively to the asymmetric and symmetric P-O-P stretching vibrations. These bands are characteristics of the P_2O_7 group [93].

The deformation vibrations of the P_2O_7 group appear as medium intensity bands in the 615-380 cm^{-1} range. In the IR spectrum of anhydrous $NaYbP_2O_7$ obtained at 500 ^oC, similar vibrational bands were observed for P_2O_7 group. But the characteristic bands belong to crystalline water became quite weak.

Hydrated $NaYbP_2O_7$

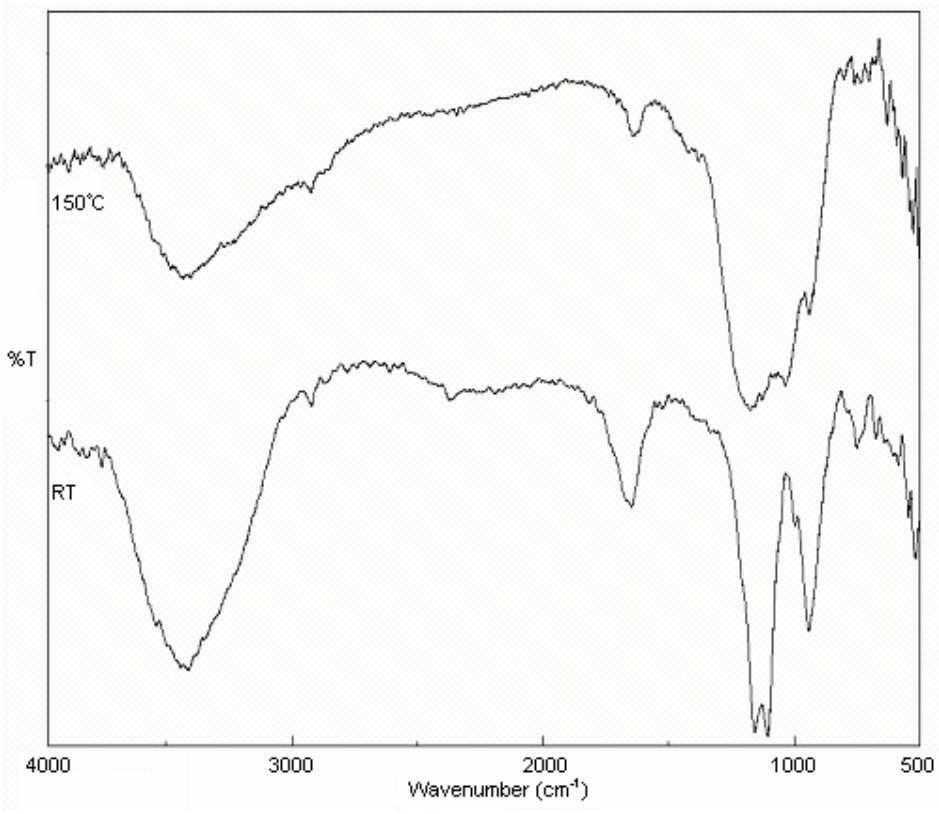

Dehydrated $NaYbP_2O_7$

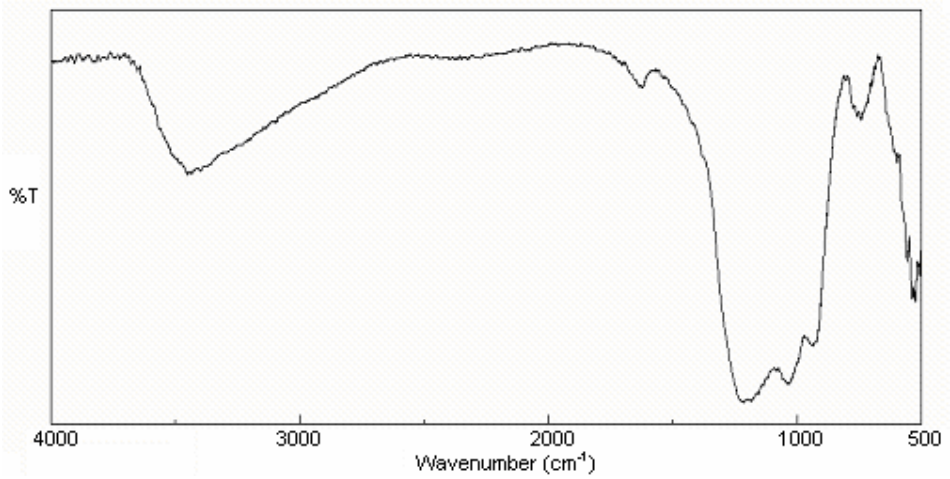

Figure 3.23. *IR Spectra of hydrated and dehydrated $NaYbP_2O_7$ at different temperatures.*

3.2. Solid State Reactions for the Synthesis of Some New Rare Earth Borophosphates Using Ln_2O_3 (Ln: Nd, Gd, Dy, Er, Yb) + $NH_4H_2PO_4$ + B_2O_3

The stoichiometric mixtures of reactants with respect to the equation given below were heated between 600-1200^oC for about 7 hours.

The expected reaction is,

$$Ln_2O_3(s) + 4NH_4H_2PO_4(s) + B_2O_3(s) \rightarrow 2LnBP_2O_8(s) + 4NH_3(g) + 6H_2O(g)$$

3.2.1. X-ray Powder Diffraction Studies for Nd, Gd, Dy, Er and Yb Compounds

The products obtained at different temperatures were subjected to X-ray powder diffraction analysis after each heating process. The diffraction patterns observed for Gd compound are given in Figure 3.24.

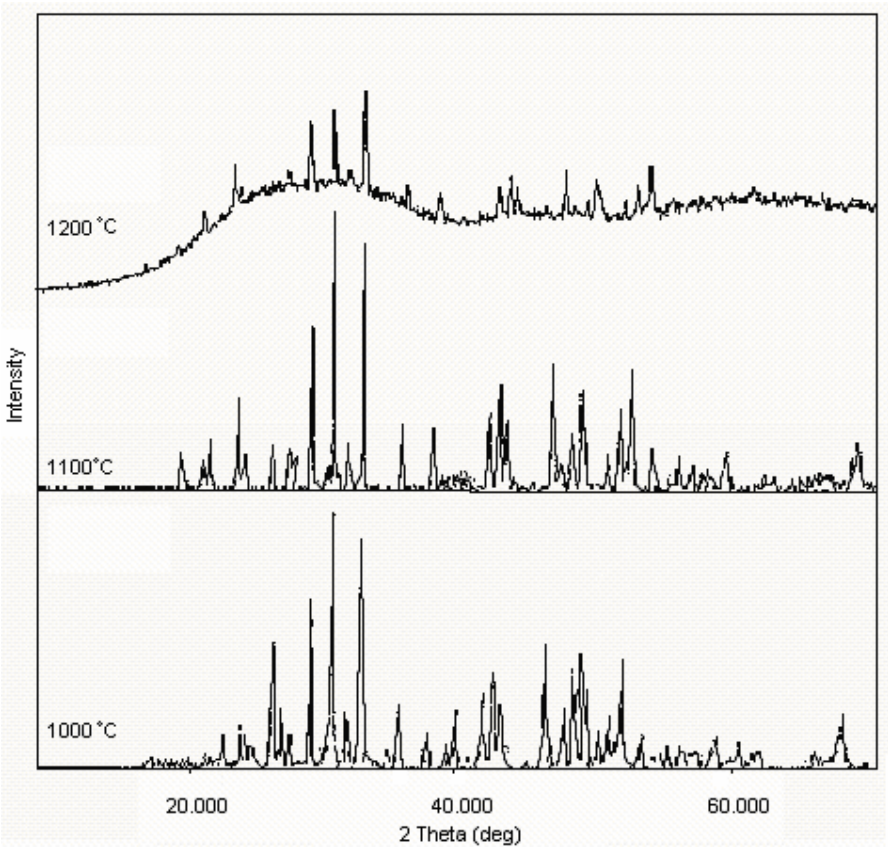

Figure 3.24. *XRD Pattern of $GdBP_2O_8$ at 1000, 1100 and 1200 ^oC.*

In the analysis of XRD patterns of the products obtained between 600-1000^{o}C unreacted Gd_2O_3 (J.C.P.D.S Card No:12-0797), $GdPO_4$ (J.C.P.D.S Card No:32-0386) and $Gd(PO_3)_3$ [73] were observed. Depending on the powder data and infrared spectra which will be discussed later, the following reaction could be considered;

$2Gd_2O_3 + 8NH_4H_2PO_4 + 2B_2O_3 \rightarrow 4BPO_4 + Gd_2O_3 + GdPO_4 + Gd(PO_3)_3 + 8NH_3 + 12H_2O$ ***(equation 1)***

At 1100 ^{o}C , examination of the XRD pattern showed that $GdPO_4$ with monazite (monoclinic) structure was found together with weak BPO_4. Since the diffraction lines belong to $Gd(PO_3)_3$ and unreacted Gd_2O_3 become quite weak.

The following reaction was suggested;

$Gd(PO_3)_3 + Gd_2O_3 \rightarrow 3GdPO_4$ ***(equation 2)***

Therefore, the final reaction could be written as follows:

$2Gd_2O_3(s) + 8NH_4H_2PO_4(s) + 2B_2O_3(s) \rightarrow 4BPO_4(s) + 4GdPO_4(s) + 8\ NH_3(g) + 12H_2O(g)$

At 1200^{o}C, since the diffraction lines for BPO_4 disappeared in the powder data, it was decided that the below reaction was produced;

$GdPO_4 + BPO_4 \rightarrow GdBP_2O_8$ ***(equation 3)***

Because of the similarities of the d-lines for the obtained compound with those of the monazite $GdPO_4$, it was predicted that the formation of monazite structure with the tentative formula $GdBP_2O_8$ or $GdPO_4.BPO_4$ was obtained.

The similar reaction pathways were found for the neodymium borophosphate. Its XRD patterns were given in Figure 3.25.

Investigation of this pattern showed that $NdBP_2O_8$ was obtained with a monazite structure at 1100°C. However, at 1200°C, it was observed that the crystalline compound transformed to the amorphous phase.

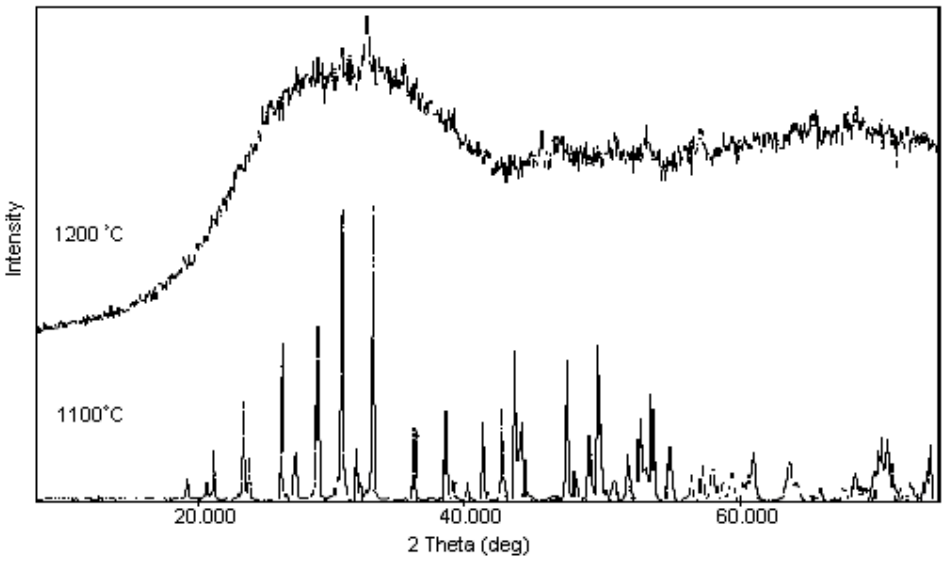

Figure 3.25. *XRD patterns for the products of* $NdBP_2O_8$ *at 1100, 1200* ^oC.

As it is known from the literature, lanthanide orthophosphates ($LnPO_4$) crystallize in two types of structures. Lanthanide elements between La and Gd crystallize with monoclinic monazite [87, 94] and from Tb to Lu with tetragonal xenotime structure. Only $DyPO_4$ crystallize in both of the structures.

When the lanthanide element was dysprosium, erbium and ytterbium, $LnBP_2O_8$ was obtained with xenotime tetragonal structure. The XRD patterns for these compounds were given in Figures 3.26, 27 and 28. Only ErB_2O_8 was indexed as shown in Table 3.10 and the unit cell parameters were calculated as a = 6.854, b = 5.999 Å.

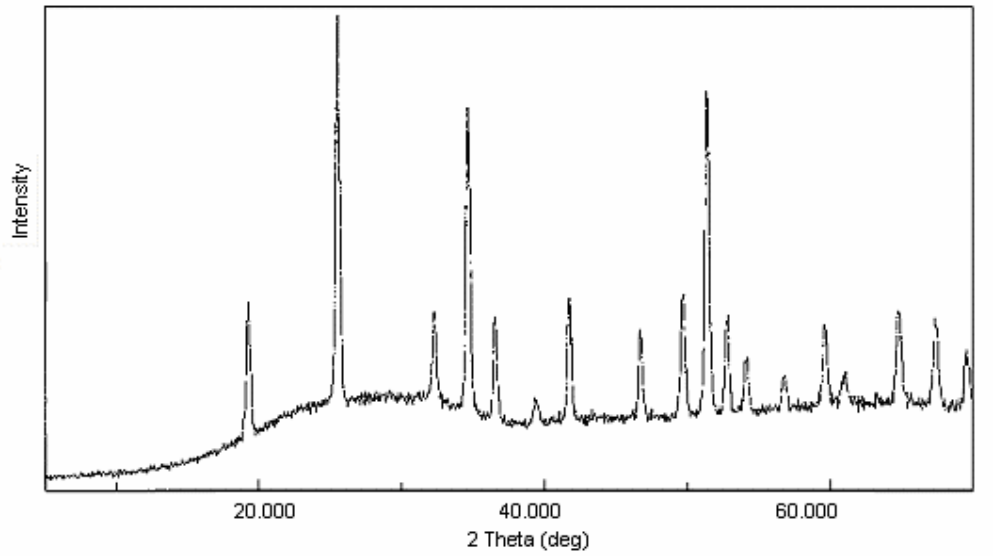

Figure 3.26. *XRD pattern for the product of* $DyBP_2O_8$ *at 1200* ^oC.

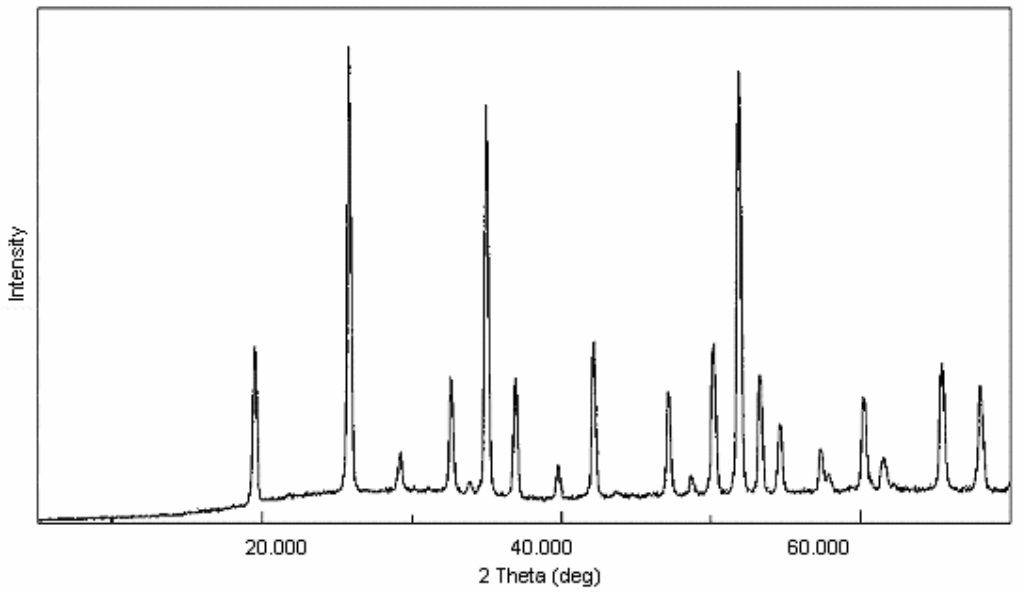

Figure 3.27. *XRD pattern for the product of* $ErBP_2O_8$ *at 1200* ^oC.

Table.3.10. *XRD data of $ErBP_2O_8$; Tetragonal With a=6,854, c=5,999 Å.*

I/I_o	d_{obs}	$d_{calc.}$	hkl
2	4.90	4.85	110
37	4.51	4.51	101
100	3.426	3.427	200
17	2.728	2.729	211
53	2.5509	2.551	112
22	2.4212	2.423	220
6	2.2575	2.257	202
26	2.1348	2.135	301
20	1.9220	1.9198	103
20	1.8124	1.8122	321
46	1.7587	1.7569	312
22	1.7143	1.7135	400
9	1.6794	1.6750	213
2	1.6010	1.6020	411
13	1.5330	1.5326	420
7	1.5043	1.5048	303
12	1.4229	1.4224	332
16	1.3766	1.3741	204

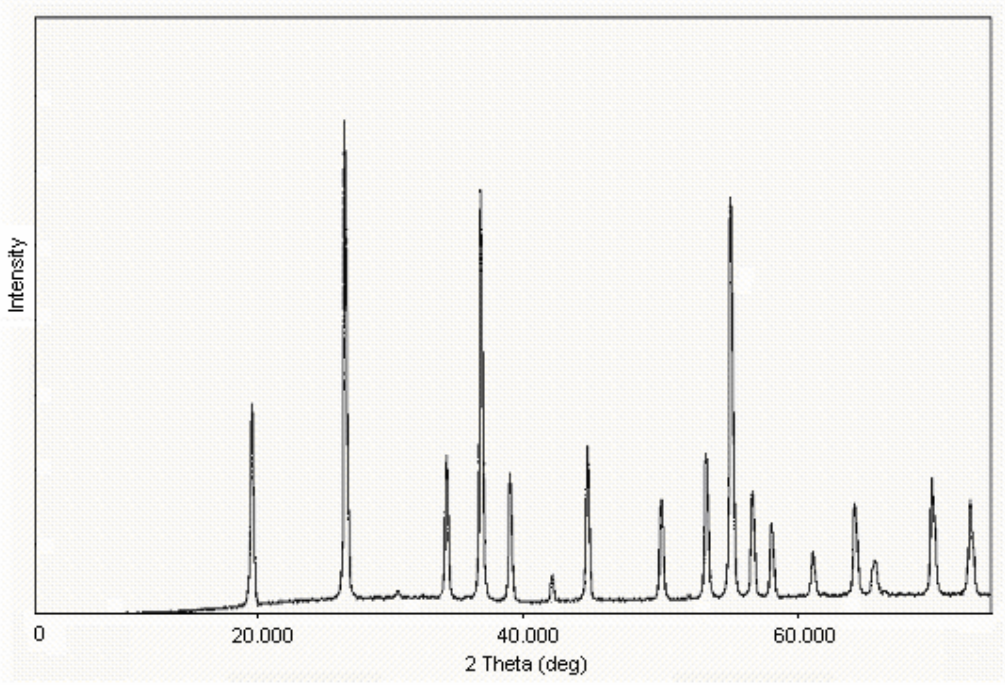

Figure 3.28. *XRD Pattern for the Product of $YbBP_2O_8$ at 1200 ^oC.*

According to the equations 1, 2 and 3 we can say that the new $LnBP_2O_8$ (Ln: Gd, Nd, Dy, Er and Yb) compounds were prepared at high temperature (after 1000°C). This results show us, Nd and Gd compounds crystallize with monazite structure; the other lanthanide compounds (Dy, Er and Yb) crystallize with xenotime structure.

3.2.2. IR Studies for Nd, Gd, Dy, Er and Yb Compounds

As shown in Figures 3.29, 30, 31, 32 and 33 infrared spectra of the products were obtained by the reactions of $Ln_2O_3 + 4NH_4H_2PO_4 + B_2O_3$ (Ln: Nd, Gd, Dy, Er and Yb) at 600- 1200°C.

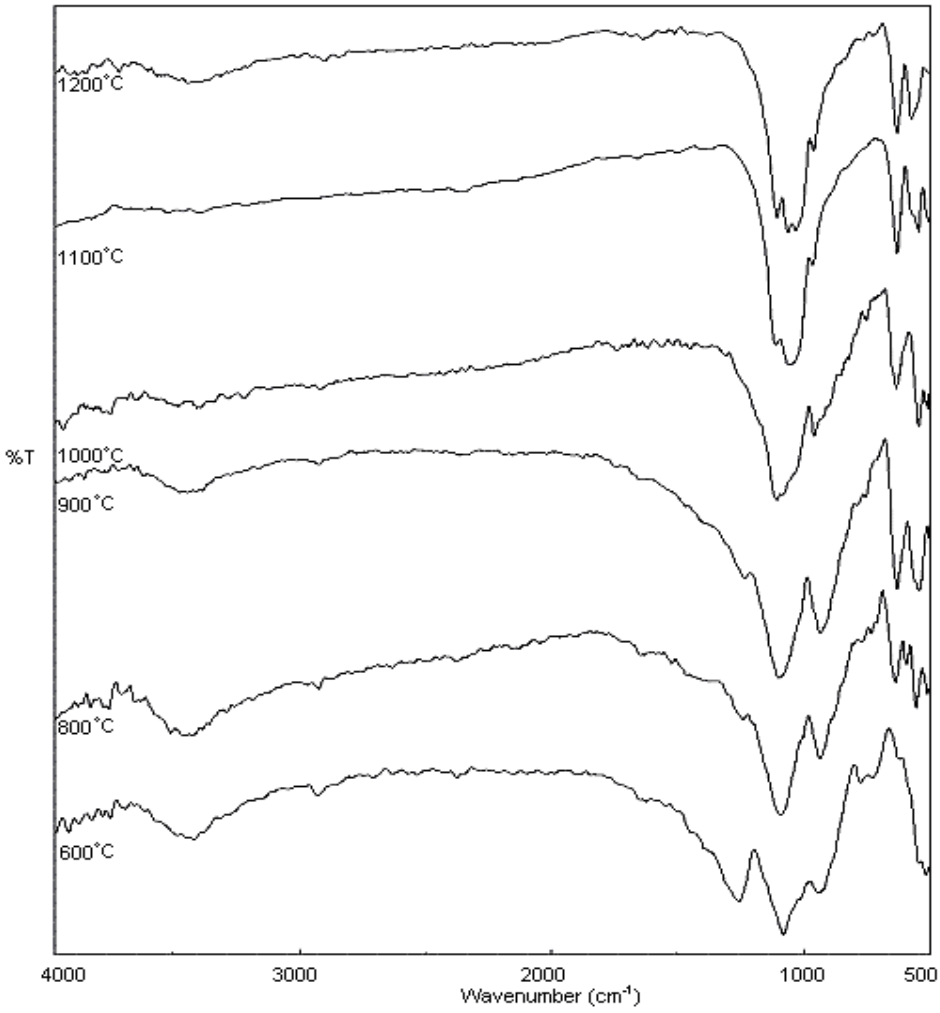

Figure 3.29. *IR Spectra of the Solid-State Reactions of $Gd_2O_3+B_2O_3+4NH_4H_2PO_4$ at 600, 800, 900, 1000, 1100 and 1200°C.*

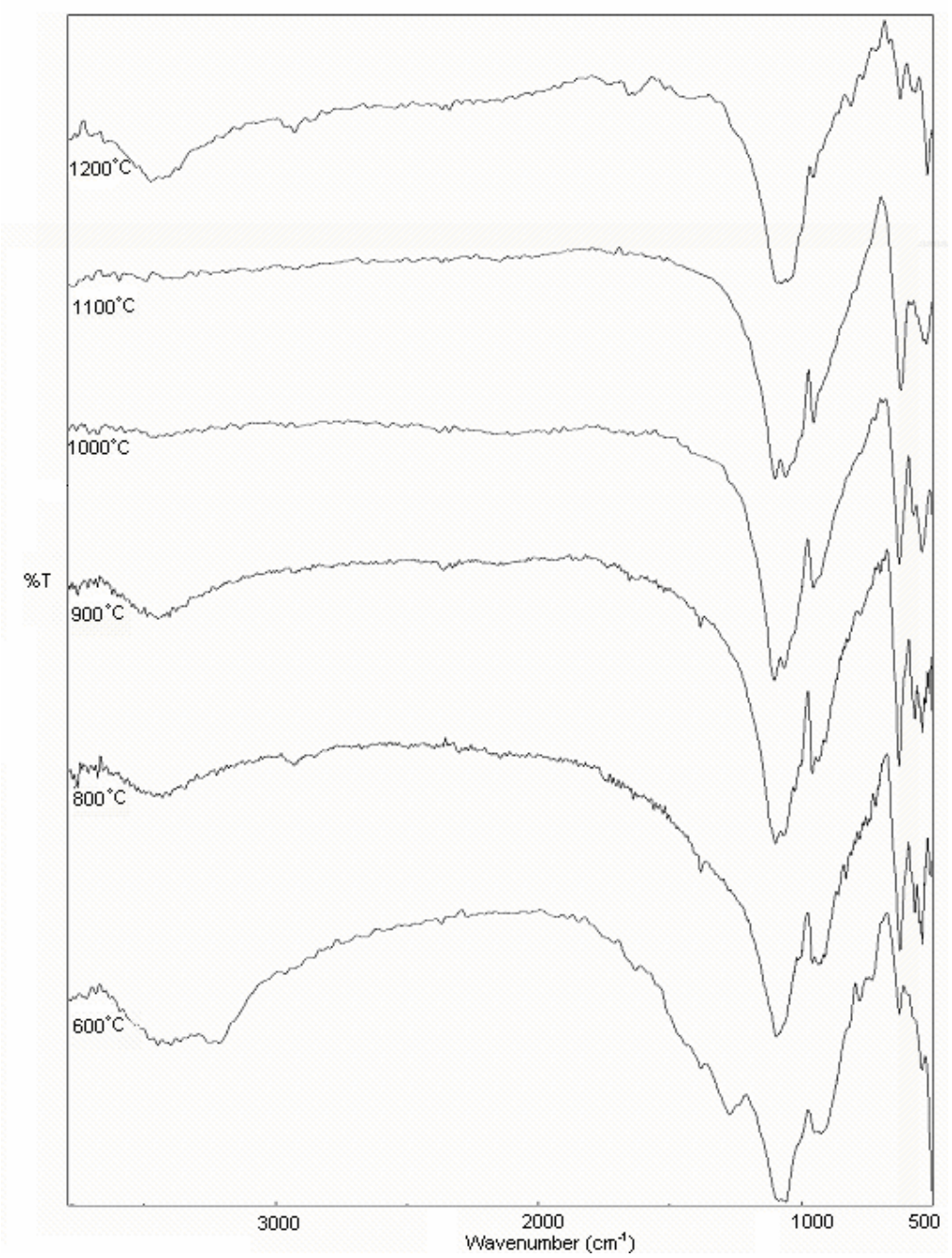

Figure 3.30. *IR Spectra of the Solid-State Reactions of* $Nd_2O_3+B_2O_3+4NH_4H_2PO_4$ *at 600, 800, 900, 1000, 1100 and 1200°C.*

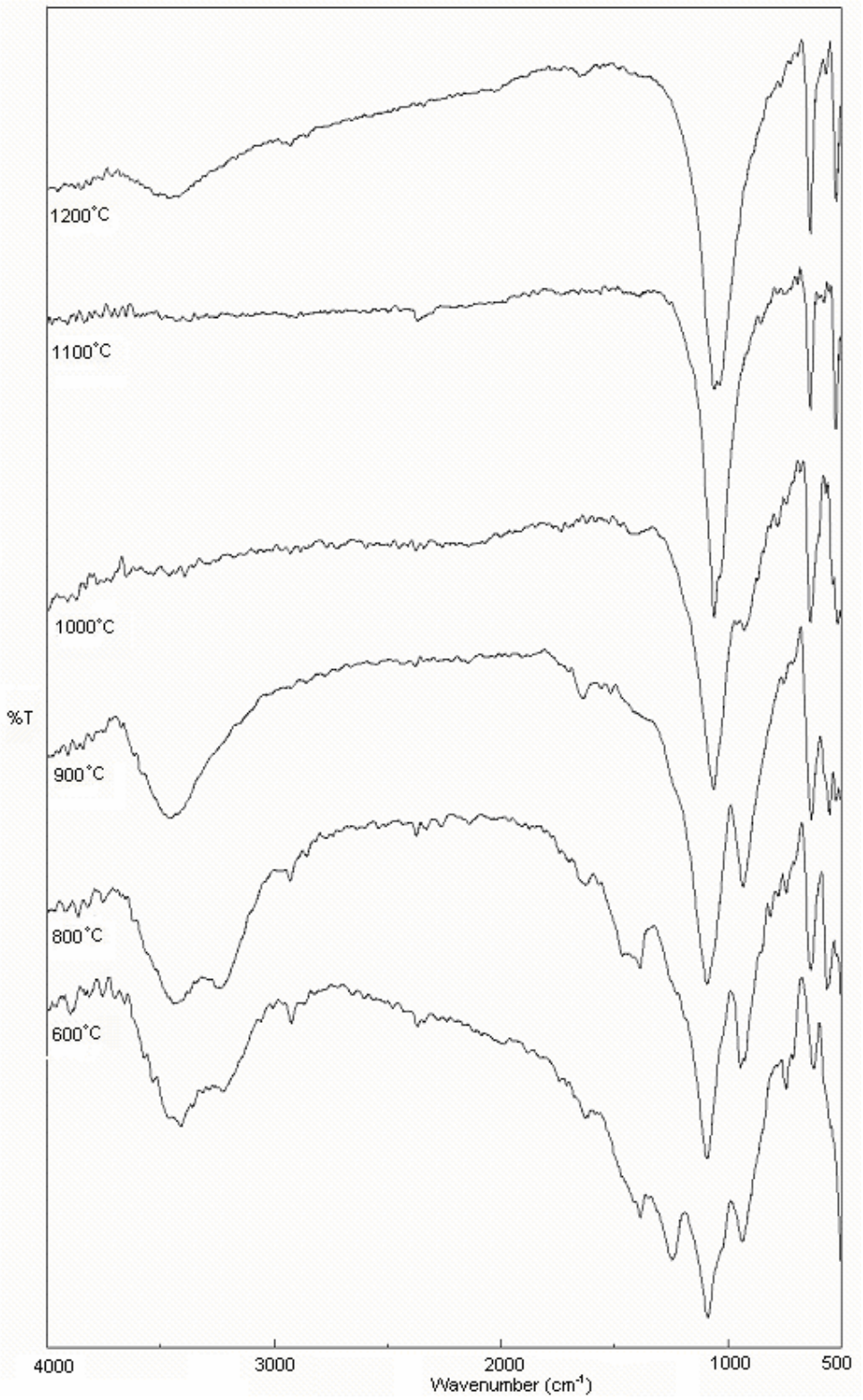

Figure 3.31. *IR Spectra of the Solid-State Reactions of $Dy_2O_3 + B_2O_3 + 4NH_4H_2PO_4$ at 600, 800, 900, 1000, 1100 and 1200^oC.*

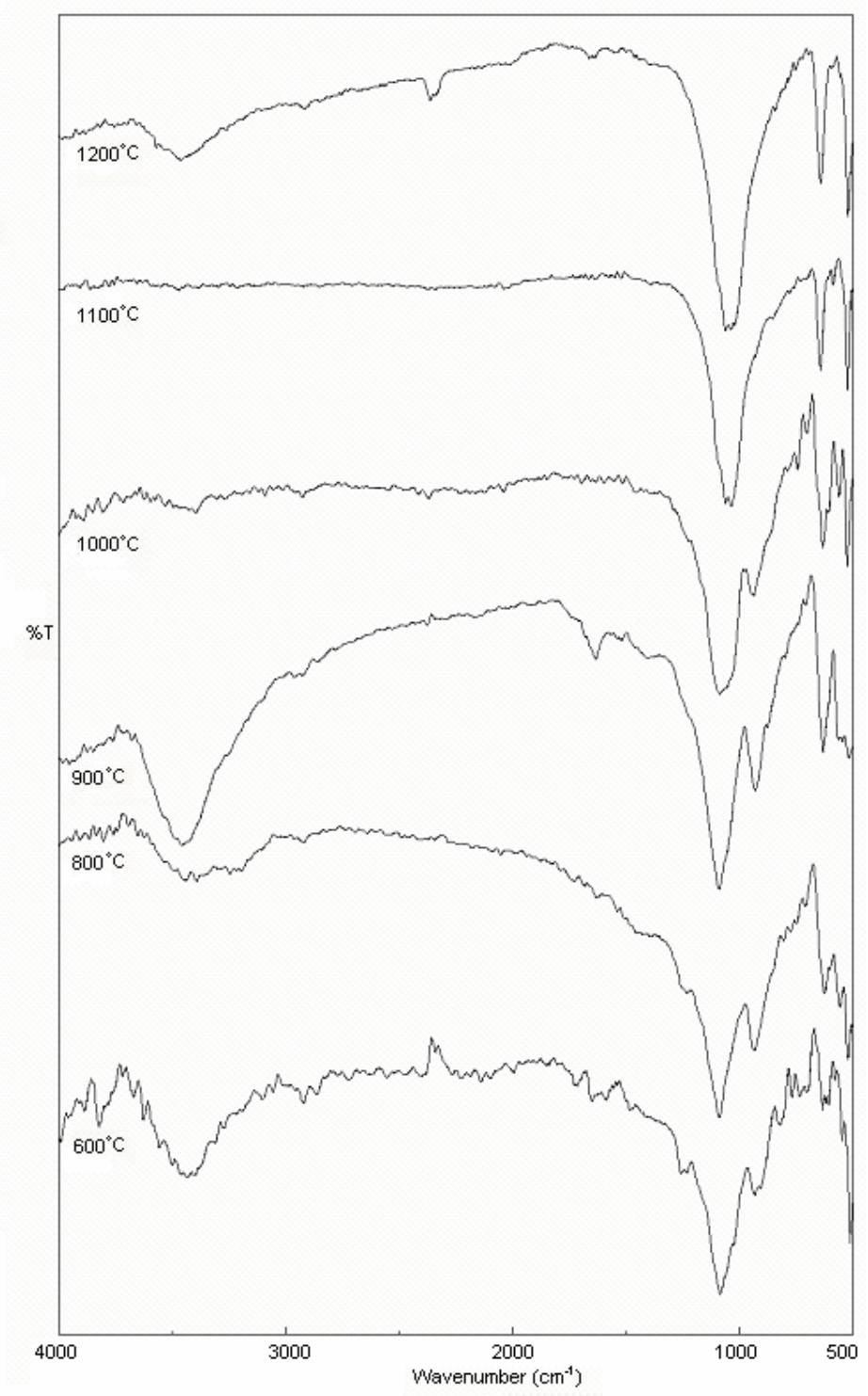

Figure 3.32. *IR Spectra of the Solid-State Reactions of $Er_2O_3 + B_2O_3 + 4NH_4H_2PO_4$ at 600, 800, 900, 1000, 1100 and 1200°C.*

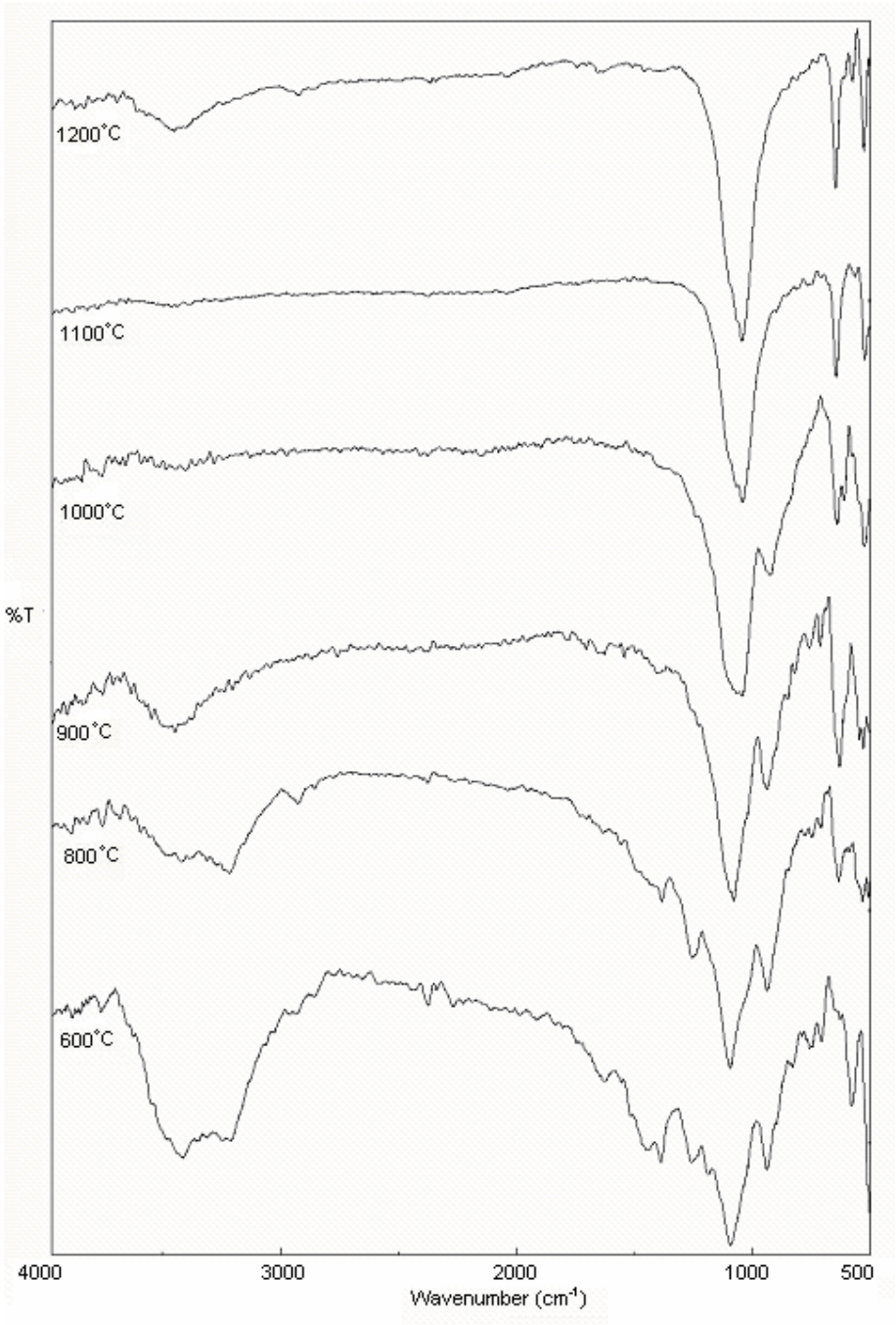

Figure 3.33. *IR Spectra of the Solid-State Reactions of* $Yb_2O_3+B_2O_3+ 4NH_4H_2PO_4$ *at 600, 800, 900, 1000, 1100 and 1200°C.*

At low temperatures (600-900^{o}C), the vibrational bands due to BPO_4, $LnPO_4$ with monazite (Ln: Nd, Gd) or xenotime (Ln: Dy, Er and Yb) structure [95], $Ln(PO_3)_3$ [73] and Ln_2O_3 [93] were observed.

At high temperatures (after 1000 ^{o}C), the IR absorbtion bands according to $Ln(PO_3)_3$ and Ln_2O_3 disappeared. Table 3.11 shows the assignment for the vibrational frequencies of the products at 1100 ^{o}C and 1200 ^{o}C.

Table 3.11. *IR Absorption Bands and Assignments for the Products Obtained from the Reaction of* $Ln_2O_3 + 4NH_4H_2PO_4 + B_2O_3$ *(Ln: Nd, Gd, Dy, Er and Er) at 1100^{o}C and 1200^{o}C.*

Frequency υ(cm^{-1})	**Assignments**
1100-1000	υ_3 PO_4
970-940	υ_3 BO_4, υ_1 PO_4
635-620	υ_4 PO_4, υ_3 BO_4
580 (weak)	υ_4 BO_4
566-525	υ_4 PO_4

CHAPTER IV

GENERAL REVIEW AND CONCLUSION

The preparation of $NaLnP_2O_7$ (Ln= La, Ce, Nd, Eu, Gd and Y) were attempted in our laboratory before through solution reactions only the synthesis of $NaNdP_2O_7$ was achieved through a solution reaction [96].

In the first part of this thesis, the synthesis of other sodium lanthanide diphosphates (Ln: Nd, Gd, Dy, Er, Yb) through the solution reaction of $LnCl_3$ with $Na_4P_2O_7$ were studied. The reaction products were examined by thermal analysis, X-ray powder diffraction and infrared spectroscopy methods.

All of the hydrated sodium lanthanide diphosphates ($NaLnP_2O_7.xH_2O$) were synthesized with 4-5 moles of water. But only $NaYbP_2O_7.xH_2O$ could be prepared as crystalline. Whereas the others were obtained as amorphous. To prepare dehydrated sodium lanthanide diphosphates ($NaLnP_2O_7$), these compounds were subsequently heated at different temperatures. $NaNdP_2O_7$ and $NaYbP_2O_7$ were obtained as real crystalline compounds. Whereas Dy and Er diphosphates were prepared pseudo-$NaLnP_2O_7$. Gd compound was decomposed to the another phosphates.

In the second part of this work, the study of preparation of $LnBP_2O_8$ (Ln: Nd, Gd, Dy, Er, Yb) through the solid state reactions of Ln_2O_3 with $NH_4H_2PO_4$ was investigated at temperatures between 600-1200^oC. Examination of the XRD and IR data showed that the reaction was not completed up to 1000^oC. After 1100^oC, the formation of monazite (Ln:Nd, Gd) and xenotime (Ln: Dy, Er, Yb) structure with the

formula of $LnBP_2O_8$ was observed. Only the XRD pattern of Er compound was indexed in tetragonal system with the unit cell parameters; a=6.854 and c=5.999 Å.

REFERENCES

[1] Giesbrecht E., and Perrier M., *Annais. Brasil de Quim. 19-20 (1960-1961) 121.*

[2] Kızılyallı M., *J.Less-Common Met. 127 (1987) 147.*

[3] Chehimi-Moumen F., Ben Hassen-Chehimi D., Ferid M., Trabelsi-Ayadi M., *Mater. Res. Bull. 36 (2001) 365.*

[4] Chehimi-Moumen F., Ben Hassen-Chehimi D., Ferid M., Trabelsi-Ayadi M., *Mater. Res. Bull. 36 (2001) 2175.*

[5] Ben Moussa S., Sobrados I., Iglesias J.E., Trabelsi Ayadi M., Sanz J., *J. Master. Chem. 10 (2000) 1973.*

[6] Tannaev I.V., and Vasil'eva V.P., *Russ. J. Inorg. Chem. 9 (1964) 1141.*

[7] Kuznetsov V.G. and Vasil'eva V.P., *Inorg. Mater. 3 (1967) 316*

[8] Tannaev I.V., Kuznetsov V.G. and Vasil'eva V.P., *Inorg. Mater. 3 (1967) 87.*

[9] Anisimova N.Yu., Trunov VK. and Chudinova N.N., *Izv.Akad.Nauk SSSR, Neorg. Mater. 24-2 (1988) 286.*

[10] Kızılyallı M. and Darras M. *J.Solid-State Chem. 107 (1993) 373.*

[11] Ferid M., Horchani K., Amami *J*., *Mater. Res. Bull. 39 (2004) 1949.*

[12] Ferid M., Horchani-Naifer K., *J*., *Mater. Res. Bull. 39 (2004) 2209.*

[13] Tie S.L., Li Y.Y., Yang Y.S., *J. Phys. Chem. Solids 58 (1997) 957.*

[14] Khay N., Ennaciri A., *J. Alloys and Comp. 323-324 (2001) 800.*

[15] Kniep R., Gözel G., Eisenmann B., Röhr C., Asbrand M. and Kızılyallı M. *Angew. Chem. Int. Ed. Engl. 33 (7) (1994) 749.*

[16] Gözel G. *"Preparation and Structural Investigation of Alkaline-Earth Borophosphates" , Ph. D. Thesis, METU, Ankara 1993.*

[17] Sedmale G., Vaivads J., Sedmalis U., Kabanov V.O., and Yanush O.V., *Journal of Non-crystalline Solids 129 (1991) 284.*

[18] Shi Y., Liang J.K., Zhang H., Liu Q.L., Chen X.L., Yang J.L., Zhuang W.D., and Rao G.H, *Journal of Solid State Chemistry 135 (1) (1998) 43.*

[19] Pushcharovsky D.Yu., Gobetchia E.R., Pasero M., Merlino S. and Dimitrova O.V. *J. of Alloys and Comp. 339 (2002) 70.*

[20] Bontchev P.B. and Sevov S.C., *Inorganic Chemistry 35 (1996) 6910.*

[21] Velsko S.P., Webb M., Davis L. and Huang D., *IEEE J.Ouant. Electron 27 (1991) 2182.*

[22] Chen C., Wu Y. and Li R., *Journal of Crystal Growth 99 (1990) 790.*

[23] Fan T.Y., Huang C.E., Hu B.Q., Eckhardt R.C., Fan Y.X., Bayer R.l. and Feigelson R.S., *Appl. Opt. 26 (1987) 2391.*

[24] Baykal A., Gözel G., Kızılyallı M., Toprak M. and Kniep R., *Turkish J. Chem. 24 (2000) 381.*

[25] Baykal A., "Synthesis and Characterization of Alkaline Earth and Rare Earth Borophosphate Compounds" Ph.D. Thesis, Chemistry Department, METU, Ankara, Turkey, May (1999).

[26] Baykal A., Kızılyallı M., Gözel G., and Kniep R., *Cryst. Res. Technol. 35 (3) (2000) 247.*

[27] Yılmaz A., Bu X.H., Kızılyallı M., Kniep R., and Stucky G.D., *J. of Solid State Chem. 156 (2) (2001) 281.*

[28] Gözel G., Baykal A., Kızılyallı M., and Kniep R., *J. of the Eur. Cer. Soc. 18 (1998) 2241.*

[29] Wu Y., Wang G., FU, P., Liang X., Xu Z., and Chen C., *J of Crystal Growth 229 (2001) 205.*

[30] Baykal A, Kızılyallı M., *J. of Mat. Science 35 (2000) 4621.*

[31] Breck D.W., *Zeolite Molecular Sieves, Wiley & Sons, Newyork, (1974).*

[32] Gier T.E., Stucky G.D., *Nature(London) 349 (1991) 508.*

[33] Wilson S.T., Lok B.M., Messina C.A., Cannon T.R., Flanigen E.M., *J. Chem. Soc. Chme. Commun. 104 (1982) 1146.*

[34] Behrens P., Stucky G.D, Albert G., and Bein X., *In Comprehensive Supramolecular Chemistry 7 (1996) 721.*

[35] Kniep R., Schafer G., Engelhardt H., Boy I., *Angew Chem. Int. Ed. 38 (1999) 3642*.

[36] Yılmaz A., Bu X.H, Kızılyallı M., and Stucky G.D., *Chem. Mater. 12 (2000) 3243.*

[37] Grimmer A.R, Müller D., Gözel G., and Kniep R., *Fresenius J. of Analy. Chem. 357 (1997) 485.*

[38] Shi Y., Liang J., Zhang H., Yang J., Zhuang W., and Rao G., *J. of Solid State Chem. 129 (1997) 45.*

[39] Kniep R. Gözel G., Eisenmann B., Röhr C., Asbrand M., Kızılyallı M., *Angew Chem. 106 (1994) 791.*

[40] Liebau F., *Structural Chemistry of Silicates, Springer Verlag, Heidelberg (1985).*

[41] Kniep R., Engelhardt H., Hauf C., *Chem. Mat. 10 (1998) 2930.*

[42] Bluhm K., and Park C.H., *Zeitschrift für Naturforschung, 52b (1997) 102.*

[43] Tarte P., and Schroder U.W., *C.R., Acad. Science of Paris II, 295 (1982) 351.*

[44] Bluhm K., and Park C.H., *Zeitschrift für Naturforschung, 50b (1995) 1617.*

[45] Hutchings G.J., Hudson I.D., and Timms D.G., *J. of Chem. Commun. 23 (1994) 2717.*

[46] Vasovic D.D., Stojakovic D.R., and Zec S.P., *Mat. Res. Bull. 32 (6) (1997) 779.*

[47] Schueller K.H., *Ber. Deu. Keram. Ges. 44 (6) (1967) 284.*

[48] Croop E.J., and Vondracek C.H., *Westinghouse Electric Corp. Pat:Fr., 1 (c1. c01b. H01b Feb. 5 (1965) 338.*

[49] Parry R., and Reid A.M., *Pat: Fr., 1, 359,103(c1, c08c), April 24.*

[50] Kumta P.N., Sriram M.A., *J. of Material Science 28 (1993) 1097.*

[51] Hsu R., and Kumta P.N., *J. of Material Science 30 (1995) 3123.*

[52] Hsu R., Kim J.Y., Kumta P.N., and Feist T.P., *Chemistry of Materials 8 (1996) 107.*

[53] Baykal A., and Kızılyallı M., *J. of Chemical Eng. Turkey, (1997) 152.*

[54] *Nat.Bur. Stand.(U.S) Monogr. 25 (20) (1983) 23.*

[55] Dachille F., and Dent-Glasser L., *Acta Crystallogr. 12 (1959) 280.*

[56] Goltz H., and Moffat J.B., *Journal of Catal. 22 (1971) 85.*

[57] Baccaredda H.L., Neucetti G.F., and Tartarelli R., *Chim. Ind. Milan. 45 (1963) 1483*.

[58] Yılmaz A., *Master Thesis, Chemistry Dept. of METU, Ankara, (1995).*

[59] Toprak M., *Master Thesis, Chemistry Dept. of METU, Ankara, (1996).*

[60] Ray N.H., *Inorganic Polymers, London, Academic Press, (1978).*

[61] Mingos D.M.P and Baghurst D.R., *Chem. Soc. Rev. 20 (1991) 1.*

[62] Roy R., Komarneni S., and Yang L.J., *J. Am. Cer. Soc. 68 (7) (1985) 392.*

[63] Sutton W.H., *Ceramic Bulletin 68 (2) (1989) 376.*

[64] Kamo M., Sato Y., Matsumoto S., and Setaka N., *J Cryst. Growth 62 (3) (1983) 642.*

[65] Hauf C., Yılmaz A., Kızılyallı M., and Kniep R., *J. Solid State Chem. 140 (1998) 154.*

[66] Hauf C., Friedrich T., and Kniep R., *Z. Kristallogr. 210 (1995) 446.*

[67] Vaidhyanathan B., and Rao K.J., *J. Solid State Chem. 132 (1997)349.*

[68] Vaidhyanathan B., and Rao K.J., *Chem. Mater. 9 (1997) 1196.*
,
[69] Baykal A., Kızılyallı M., Toprak M., and Kniep R., *Turkish J. Chem. 25 (2001) 425.*

[70] Bor Madenleri, *DPT–2123, OIK–327, Mart 1988*

[71] Türkiye Bor Mineralleri Envanteri, *MTA, no:162, Ankara, 1976.*

[72] Notholt A.J.G, P*hosphate Rock in the CENTO Region (Iran, Pakistan and Turkey), CENTO, Ankara, 1977.*

[73] Uztetik A., *Ph.D Thesis, Middle East Technical University, Ankara, Turkey 1992*.

[74] Aldred A.T., *Acta Cryst. B40, (1984) 569.*

[75] Corbridge D.C.,and Lowe E.J., *J. Chem. Soc., (1954) 4555.*

[76] Corbridge D.C., Grayson M., and Griffith E.J., *Topics in Phosphorus Chemistry, vol 3, Inters cience, New York, 1961, p.235.*

[77] Harwey R.B., and Mayhood J.E., *Can. J. Chem. 33 (1955) 1152.*

[78] Palmer W.G., *J. Chem. Soc. (1961) 1552.*

[79] Harcharras, M., Ennaciri A., Khay N., and Brouzi K. *Phosphorus, sulfur and silicon 178 (2003) 1247.*

[80] Brouzi K. Ennaciri A., and Harcharras, M., *Phosphorus, sulfur and silicon 179 (2004) 1239.*

[81] Hezel A. and Ross, S.D., *Spectrochim. Acta. Part. A23, (1967) 1583.*

[82] Cornilsen B.C., and Condrate R.A, *J. Phys. Chem. Solids 38 (1977) 1327.*

[83] Cornilsen B.C., and Condrate R.A, *J. Solid State Chem. 23 (1978) 375.*

[84] Cornilsen B.C., *J. Mol. Struct. 117 (1984) 1.*

[85] Walrafen G.E., Irish D.E., and Young T.F., *J. Chem. Phys. 37 (1962) 662.*

[86] Khay N., Ennaciri A., and Harcharras M., *Vibr. Spectrosc. 27 (2001) 119.*

[87] Kızılyallı M., and Welch A.J.E., *J. Appl. Cryst. 9 (1976) 413.*

[88] Kızılyallı M., *J. Inorg. Nucl. Chem. 1 (1975) 1406.*

[89] Tananev I. V., Kuznetsov V.g. and Petushka S. M., *Russ. J. Inorg. Chem. 11 (1996) 286.*

[90] Uztetik-Amour A., and Kızılyallı M., *High Temp. and Mater. Sci. 36 (1996) 77.*

[91] Robertson B.E., and Calvo C., *J. Solid State Chem. 1 (1970) 120.*

[92] Tondon V.K., and Calvo C., *Indian J. Pure Ap. Phy. 19 (1981) 756.*

[93] Rulmont A., Cahay R., Liegeois-Duyckaerts M., and Tarte P.,*Eur. J.Solid State Inorg. Chem. 28 (1991) 207.*

[94] Kızılyallı M., *The Chemistry and Structure of Rare Earth Phosphates, PhD Thesis, London University,(1973).*

[95] Ross S.D., *Inorganic Infrared and Raman Spectroscopy, Mc Graw Hill Book Company (UK), 1972.*

[96] Uztetik-Morkan A., Morkan İ., Özen G., Güler H., and Kızılyallı M. *Phosporus, Sulfur and Silicon 180 (2005) 2635.*